Minor and Trace Element and Re-Os Chemistry of the Upper Devonian Woodford Shale, Permian Basin, West Texas: Insights into Metal Abundance and Basin Processes

Nicholas B. Harris[a,b], Cheryl A. Mnich[b,c],David Selby[d] and Dieter Korn[e]

[a]Department of Earth and Atmospheric Sciences, University of Alberta, 1-26 ESB, Edmonton, Alberta, CANADA T6G 2E3, nharris@ualberta.ca

[b]Department of Geology and Geological Engineering, Colorado School of Mines, Golden CO 80401, U.S.A.

[c]Now at: ConocoPhillips (United Kingdom), Rubislaw House, Anderson Drive, Aberdeen AB15 6FZ, Scotland, cheryl.mnich@conocophillips.com

[d]Department of Earth Sciences, Durham University, Durham DH1 3LE,UK, david.selby@durham.ac.uk

[e]Museum für Naturkunde, Leibniz Institute at the Humboldt University Berlin, Invalidenstraße 43, D-10 115, Berlin, Germany, dieter.korn@mfn-berlin.de

ABSTRACT

The trace and minor element and Re-Os geochemistry of the Upper Devonian Woodford Shale are analyzed in order to characterize elemental abundances, identify associations among trace elements and to constrain paleoceanographic conditions and depositional processes. This

organic-carbon-rich mudstone in the Permian Basin, west Texas, is a major source of hydrocarbons in the basin and is coeval with many other Upper Devonian shales in North America.

The Woodford lacks enrichment in many trace metals. Only Mo, U, S and Se are significantly enriched. Other redox sensitive elements are depleted or similar to average shale composition, including Pb, Bi, Cr, Ti, Cu, Zn, Co, and V. Elements associated with granitic sources such as rare earths, Th, Ce, and TiO_2 are also depleted relative to average shale; this appears to be related to be a source control. A strong basin reservoir effect is noted among several redox sensitive elements, including Mo, Cu and Ni, which largely accounts for the depletion. Dilution by biogenic silica had an additional effect on metal concentrations. Multivariate factors analysis identified associations between elements, including groupings of: rare earth elements; elements enriched in granitic crust; silica, varying antithetically with elements in carbonate minerals; organic carbon, Mo and U; V; phosphate; Fe and S. Noteworthy among the results are the different behavior of redox-sensitive elements, suggesting different precipitation mechanisms or varying dependence on reservoir effects.

A strong redox effect is noted in the TOC/P_{tot} ratio at approximately the Frasnian – Famennian boundary, indicating an abrupt transition to an anoxic column boundary that coincides with a short-term significant fall in sea level. This suggests that anoxia was induced by isolation of the basin from the global ocean. However with the exception of the uppermost Famennian, initial $^{187}Os/^{188}Os$ values determined from Re-Os geochronology for the Permian Basin are similar to

correlative sections of the Appalachian and Peace River Basins of North American and the Rhenohercynian basin of Europe. This indicates that although the Permian Basin became restricted during the upper Devonian and early Mississippian, ocean connectivity remained between regional and global basins.

1. Introduction

Organic-carbon-rich mudstones, so-called 'black shales', are generally regarded as enriched in many trace metals and, in fact, are significant economic resources of U, Mo, Ni, Mn, V, Hg, Sb, Au, and W. Enrichment results from the potent reduction capacity associated with high reactive organic carbon content and the decreased solubility and increased reactivity of metals under reducing conditions; organic matter also provides reaction pathways for fixing metals. However, metal abundance in mudstones also depends on sources of metals, which may be derived from the global ocean through hydrothermal processes at mid-ocean spreading centers or from detrital or chemical weathering and transport from continental sources. Where exchange of water masses between a basin and the global ocean is restricted, possibly the case in some black shale basins, that may be indicated by anomalously low trace metal concentrations.

We examine trace element abundances and associations in the Woodford Shale, an Upper Devonian to Lower Mississippian organic carbon-rich mudstone in the Permian Basin, west Texas. The Late Devonian was noteworthy both for the global deposition of organic-carbon-rich

67 shales (Figure 1A) and for instability in a number of marine geological and geochemical
68 parameters. It includes the famous Frasnian – Famennian boundary, which marks one of the
69 great extinction events in the Phanerozoic (Hallam and Wignall, 1997), although Schindler
70 (1993) noted that the 'crisis' may in fact comprise a series of extinctions spaced over a period of
71 one million years. Geochemical fluctuations have been documented during this time, including
72 positive perturbations of +4 to +6 ‰ in $\delta^{13}C_{carb}$ (Saltzman, 2005), interpreted to be the result of
73 enhanced phosphate (nutrient) flux to the photic zone due to extreme anoxia. The Late
74 Devonian also had a distinctive paleogeography, with large areas of epicontinental seaways and
75 continental sags in present-day North America (Algeo et al., 2007), Europe and Australia. In this
76 configuration, even relatively small sea level fluctuations could have had a profound effect on
77 both the stratigraphy and geochemistry of sediments deposited in these basins.
78
79 In this study, we compare analyses from two long cores to average shale values to determine
80 which metals are, in fact, enriched. We then apply factor analysis, a multivariate statistical
81 technique, to the whole rock geochemical data to identify associations between elements that
82 aid in interpretations of redox conditions, metal fixation and metal sources. Factor analysis
83 seeks to reduce the dimensionality of a data set by finding associations among the original
84 variables (Howarth and Sinding-Larson, 1983; Swan and Sandilands, 1995), which here are the
85 oxide or elemental concentrations. The effect is to explain much of the variance in the original
86 data set with a greatly reduced number of new variables, termed factors.
87

Finally we examine stratigraphic patterns in trace element concentrations and Re-Os geochemistry, which provide insight into the temporal evolution of oceanographic processes such as mixing and renewal of water masses in the Late Devonian Permian Basin. We also test whether the trace element patterns can provide the basis for stratigraphic correlation between different sites within the basin.

2. Geology of the Woodford Shale, Permian Basin

The Permian Basin during the Late Devonian occurred on the southern margin of the Euramerican continent, facing the Rheic Ocean (Figs 1A and 1B). The basin was bounded to the north by the Pedernal Massif, a Precambrian siliciclastic terrane (Mukhopadhyay et al., 1975) that was the only significant source of siliciclastic sediment to the basin. Carbonate platforms bounded the basin to the east, west and southwest (Comer, 1991). The eastern margin, the Concho Arch, is reasonably well-defined, but the western margin, the Diablo Platform, was subsequently tectonically dismembered, and its existence is now inferred from facies relationships (Comer, 1991; Hemmesch et al., in press). The connection to the Rheic Ocean must have lain between the Concho Arch and Diablo Platform, but evidence for this was obscured by later development of the Ouchita-Marathon Fold-Thrust Belt and the Southern Shelf. Post-Devonian tectonics also reconfigured the interior architecture of the basin. Specifically, the Central Basin Platform is a late feature that did not impact Devonian sedimentation but did result in shallower burial depths and distinctly lower thermal maturities for this section on the platform.

The Woodford Shale in the Permian Basin, west Texas (Fig. 1C), first described by Ellison (1950), is one of several Upper Devonian shale formations in North America; others include the Marcellus and overlying shales in the Appalachian Basin, the Bakken Shale in the Williston Basin, the Antrim Shale in the Michigan Basin and the New Albany Shale in the Illinois Basin (Figure 1B). Unlike most of these other formations, which were deposited in relatively short time intervals, the Woodford represents deposition during a long (30 Myr) and apparently continuous time interval and is dated as uppermost Givetian to lowermost Mississippian (Comer, 1991; Meyer and Barrick, 2000; Hemmesch et al., in press). Interpretations of eustatic sea cycles during this time differ. Haq and Schutter (2008) documented a second order fall in sea level of approximately 70 m during this time, but Algeo et al. (2007) and references therein describe a second order rise in sea level from the late Eifelian to the late Frasnian (Johnson et al., 1985) or late Famennian (Algeo et al., 2007) or latest Famennian (Savoy and Mountjoy, 1995).

The Woodford Shale is noteworthy for its high organic carbon content (Comer, 1991; Harris et al., 2009; Hemmesch et al., in press). The Woodford is also noteworthy for high gamma ray values (Comer, 1991) that correlate closely with TOC content, commonly in the range of 300-400 API units and locally up to 800, which are used to subdivide the formation into upper, middle and lower units (Figure 2; Comer, 1991). The non-organic fraction of the mudstones consists of biogenic and detrital quartz, subordinate clay and minor feldspar; it is locally

enriched in dolomite or phosphate (Mnich, 2009; Harris et al., 2009). Pyrite averages 3 weight % and is found as nodules, euhedral crystals, and framboids (Mnich, 2009; Poole et al., 2010).

Smaller scale cycles can be recognized in the Woodford Shale cores (Hemmesch et al., in press). In the Pecos County well, these cycles are 5 to 13 meters thick and are manifested by intervals in which carbonate beds are common, separated by intervals in which carbonate beds are absent. Carbonate beds are unambiguously interpreted as turbidites; they fine upward subtly at the tops of beds, commonly display parallel lamination, and the thickest beds contain rip-up clasts of organic-carbon-rich mudstone. At least 11 such cycles were identified in the Pecos Count well, indicating that these reflect 3rd order sea level cycles; carbonate-rich intervals are interpreted to be high stand systems tracts, whereas the intervals lacking carbonate beds are interpreted to be the falling stage, low stand and transgressive systems tracts. The Winkler County well, located in the basin center (Fig.1C), lacks the common carbonate beds; here, cycles are typically 30 meters thick and represented by intervals containing abundant mm-scale radiolarian-rich laminae, separated by intervals with few or no such laminae. These are also interpreted to reflect 3rd order sea level cycles, where the intervals with abundant radiolarian laminae correspond to low stand systems tracts.

3. Methods

3.1 Sampling

Our dataset represents detailed sampling of two long Woodford cores: the RTC #1 core from the Pecos County in the western Permian Basin (103.46°W, 30.79°N); and the KCC 503 core from Winkler County on the Central Basin Platform (102.97°W, 31.89°N) (Figs. 1 and 2). The Pecos County core is from a depth of 3890 to 3990 meters and represents almost the entire thickness of the formation (Fig. 2A). The Winker County core is from 2515 to 2608 meters and covers the Middle and the lowermost part of the Upper Woodford (Figure 2B).

Cores samples, taken every 1.3 to 1.5 meters and representing 5 to 15 cm of stratigraphic section, were ground and homogenized. Splits of these samples were analyzed for total organic carbon (TOC), Rock-Eval parameters, minor and trace elements and organic petrology.

3.2 Rock-Eval, Organic Petrology, and ICP-MS

One hundred sixty-six samples from the Pecos County well and 180 samples from the Winkler County well were analyzed for Rock-Eval parameters and TOC. The former set was analyzed by Baseline Resolution, Inc. Analytical Laboratories, using standard Rock-Eval 6 instrumentation to determine their S1, S2, S3 and Tmax values, from which hydrogen index (HI) and oxygen index (OI) were calculated (Tissot and Welte 1984). The latter samples were analyzed using by Weatherford Labs using the Source Rock Analyzer, which yields similar parameters. Total organic carbon (TOC) in both sample sets was analyzed by Leco instrumentation.

Twenty-five samples from the Pecos County well were selected for organic petrologic analysis. Organic matter was studied under reflected light at a magnification of 500x using polished mounts of crushed whole-rock samples. Identification of different types of organic matter was

made on the basis of morphology and reflectance. The mounts were examined systematically and all types of organic matter present were noted and tallied. Tallies were then used to calculate the ratio of terrigenous-derived particles to marine-derived particles.

Seventy-five samples from the Pecos County well and 73 samples from the Winkler County well were chosen for whole-rock major, minor, and trace element analysis. Acme Analytical Laboratories Ltd. prepared and analyzed the samples using Inductively Coupled Plasma (ICP) and ICP-Mass Spectrometry (ICP-MS) and Leco (for Total C and Total S) for 60 major, minor and trace elements. Sample preparation included pulverizing samples until 85% of the material passed through a 200 mesh (74μm). One split was analyzed by ICP for major oxides, following lithium borate fusion and dilute acid digestion. Two splits were analyzed by ICP-MS for 45 trace elements; rare earths and refractory elements were determined from a lithium borate fusion and dilute acid digestion, while precious metals plus As, Bi, Cd, Cu, Hg, Mo, Ni, Pb, Sb, Se, Tl and Zn, were analyzed following an aqua regia digestion. end dissolving the crushed material for ICP-MS using lithium metaborate/tetraborate fusion and dilute nitric acid (Acme Analytical Laboratories Ltd., 2013).

Standards for the ICP and ICP-MS analysis were internal Acme Analytical Laboratories standards SO-18 for silicate-rich rocks including major oxides, rare earths and some metals, DS7 and OREAS45PA for trace metals, and CSC and OREAS76A for total S and C. Certified analytical results for these standards were determined by round robin analysis and are available from Acme (Acme Analytical Laboratories, personal communication, 2013). Results of replicate analyses of standards are included in the supplementary material for this paper.

As an external check on the accuracy of the geochemical data, 4 of the 75 samples from the Pecos County well were re-sampled from the powders returned by Acme and sent back for re-analysis as blind duplicates. Results of the replicate analyses are included in the supplementary material for this paper.

3.3 Rhenium-osmium analysis

Rhenium-osmium (Re-Os) elemental abundances and isotope compositions were obtained for four sample sets from the Pecos County core (3972.84-3973.1 m; 3944.14 – 3944.41 m; 3912.15 – 3912.38 m; 3889.53 – 3889.83 m). The sets were selected to obtain a wide stratigraphic range and record significant areas of chemical variation. The selected samples were devoid of any evidence of post-depositional hydrothermal alteration (filled fractures or veins). For each sample set, five to seven individual samples were polished to remove any drilling marks and to reveal complete clean and fresh surfaces. All samples were powdered in a Zr dish using a shatterbox. The Re-Os analytical protocol followed that reported by Selby and Creaser (2003 and references therein) and Selby (2007) at the TOTAL Laboratory for Source Rock Geochronology and Geochemistry at the Northern Centre for element and isotope tracing facility at Durham University. In brief, aliquants (~0.5 g) of a powdered sample were digested in a carius tube with a mixed tracer solution of ^{185}Re and ^{190}Os and 8ml of a 0.25g/g CrO_3 in 4N H_2SO_4 at 220˚C for 48 hrs. Osmium and Re were isolated using solvent extraction, micro-distillation and anion chromatography, respectively. The purified Re and Os fraction were analyzed on a ThermoElectron TRITON mass spectrometer using negative thermal ionization mass spectrometry via static Faraday collection for Re and ion-counting using a secondary electron multiplier in peak-hopping mode for Os. This study was completed during the same period as Rooney et al (2012) that reported procedural blanks of 16.8 ± 0.4 pg Re and 0.4 ± 0.1 pg Os, with a $^{187}Os/^{188}Os$ value of 0.25 ± 0.21 (1 SD, n = 4). During this period, in-house Re and Os (DROsS) solution standards yielded a running average $^{185}Re/^{187}Re$ value of 0.59772 ± 0.00172

(1 SD, n = 114) and a $^{187}Os/^{188}Os$ value of 0.16093 ± 0.00008 (1 SD, n = 36).

All uncertainties for elemental and isotope ratios presented in Table 2 were determined by error propagation of uncertainties in Re and Os mass spectrometer measurements, blank abundances and isotopic compositions, spike calibrations and reproducibility of standard Re and Os isotopic values using methods identical to previous studies (e.g., Rooney et al., 2011 and references therein).

4. Results

4.1 Organic Geochemistry

TOC contents range from 0.7 to 10.7% in the Pecos County well and from 2.5 to 14.1% in the Winkler County well (Figs. 3 and 4). Rock-Eval parameters differ significantly in the two wells: HI values are from 500 to 700 and OI values from 6 to 100 in the Winkler County well; and from 40 to 100 and 0 to 10, respectively, in the Pecos County well (Fig. 5A). Organic matter is dominated by marine sources throughout most of the section (Fig. 3), but a transition to a more terrestrial source occurs near the Middle Woodford – Upper Woodford contact between 3910 and 3915 meters in the Pecos County well.

The Pecos County core has an average Tmax of 478°C (Figure 5B), equivalent to a thermal maturity of 1.48% vitrinite reflectance using the conversion of Jarvie et al. (2001); this level of thermal maturity is generally regarded as within the wet gas window (Jarvie et. al., 2005). The Winkler County core has an average Tmax of 437°C, equivalent to a thermal maturity of 0.71% Ro (Figure 5), consistent with early oil generation.

4.2 Trace Element Enrichment Factors

Trace element abundances are described in terms of raw enrichment factors that are the ratios of the concentration for an element or oxide, divided by the average shale value (Wedepohl, 1991) for that element. Results are presented in a bar graph (Fig. 6), where the different segments of the bar represent the four quartiles of the population. We have also calculated enrichment factors for aluminum-normalized compositions, following Tribovillard et al. (2006), which compensates for dilution by carbonate or other minerals. Multipliers relating the raw enrichment factors to Al-normalized enrichment factors are provided in Table 1.

A large number of elements are depleted relative to average shale values. Strongly to moderately depleted elements include rare earths, which had median concentrations from 0.42 to 0.70 of average shale. Mn is significantly depleted, with 75% of the samples showing concentrations of 0.24 or less times the average shale. Other depleted elements include Zr, Bi, Ce, Rb, Pb, Cr, Sn and TiO_2. Dilution by organic carbon decreases concentrations of the trace elements by at most 14% and cannot account for the magnitude of depletions described here.

Elements whose median values are close to average shale included Cs, Co, Y, Be, P_2O_5, Zn, Cu and V, but the spread in the data for several of these elements is striking. Concentrations of Zn range from 0.08 to 22.6 times average shale. The median value for V is 1.34 times the average shale (slightly enriched), but the upper quartile has enrichment factors from 2.4 to 15.7 times the average shale.

Phosphate enrichment factors are similarly variable, ranging from 0.07 to 107.2 with high values restricted to the Upper Woodford where phosphate-chert nodules occur. Phosphate concentrations are commonly expressed as a ratio of TOC/P_{tot}. Most samples have ratios greater than 100; however samples with high P concentrations have TOC/P_{tot} ratios as low as 1.56 (Fig. 7). Correction of TOC for expulsion of oil or gas in the Pecos County well, the deeper and hotter of the two wells, would increase ratios by only 30 to 35%.

Four elements are strongly enriched in the samples: Mo, U, S and Se (Fig. 6). For these, the enrichment factor for 75% of the samples ranges from 6 to 20 times average shale. Calculated as Mo/Al_2O_3, Mo is less enriched than many other organic-rich shale formations. Several other elements, Cd, Ni, Ag, As, Sb, Ba and Hg, are moderately enriched. For these elements, 50% of the samples have enrichment factors of 1.6 to 3.7, but some samples in fact show depletion as much as 0.16 and 0.17 percent (As and Cd, respectively) of average shale values.

Enrichment factors are not notably increased by normalization to aluminum. The median enrichment for elements increased by an average of 19% in comparison to the non-normalized enrichment factors. The enrichment factor for sulfur decreased as a result of normalization, and the enrichment factor for Cd increased more than other elements. Enrichments generally increased most in the most depleted samples, which were also the most quartz-rich samples.

4.3 Trace Element Associations

Factor analysis defines factors that represent sets of associated variables, the latter of which in this case are individual element or oxide concentrations. Unlike correlation matrices that describe the correlation between the individual variables, factor analysis represents associations between the original variables and the calculated factors, where the strength of the association between original variables and new factors is expressed by correlation coefficients. High values indicate that much of the variance in the concentration of an element is related to a single factor. For example, K_2O has a correlation of 0.937 with Factor 1, meaning that 93.7% X 93.7% (= 87.8%) of the variance in K_2O is associated with Factor 1. We consider that correlation coefficients ≥0.80 are strong associations and that coefficients between 0.50 and 0.80 are moderate associations.

In our data set, the original set of major, minor and trace elements collapse to a set of 7 factors that explain 84.4% of the variance in the total data set (Table 2). The percentage of total

variance explained by the individual factors is shown in Table 2. The associations described by these 7 factors are described below:

Factor 1 – Strongly associated major elements are: Al_2O_3, Na_2O, K_2O, characteristic of clays and feldspars. Strongly associated trace elements are: TiO_2, Cr_2O_2, Cs, Ga, Hf, Nb, Rb, Ta, Th, and Zr. Moderately associated trace elements are: La, Ce, Pr, Nd, Pb and Bi.

Factor 2 –Strongly associated trace elements are: Y, Sm, Eu, Gd, Tb, Dy, Ho, Er, Tm, Yb and Lu (all rare earths). Moderately associated elements are: Ce, Pr, and Nd (also rare earths).

Factor 3 – Strongly associated components are: TOC, U, Mo and Ni. Moderately associated elements are: Co, As, Hg and Tl.

Factor 4 – Strongly associated components are SiO_2, MgO, CaO, MnO and inorganic carbon, and the moderately associated element Sr. SiO_2 is inversely correlated with MgO, CaO, MnO and inorganic carbon whereas the other elements are positively correlated.

Factor 5 – Strongly associated elements are: V and Cd. Moderately associated elements are: Sb, Ag and Se.

Factor 6 – Strongly associated components are: Fe_2O_3 and total S. Moderately associated elements are: As and Hg.

335

336 Factor 7 – The one strongly associated component is P_2O_5. Moderately associated elements are
337 Ag and Se.

338

339 *4.4 Trace Element Stratigraphy*

340

341 Key elements exhibit distinct stratigraphic patterns that provide insight into the
342 paleoceanographic evolution of the Permian Basin. We highlight: (1) redox proxies ratios,
343 specifically V/Al and Mo/Al, and TOC/P_{tot}; (2) the ratio of metals to TOC that may reflect
344 reservoir effects, specifically Mo/TOC, Cu/TOC, and Ni/TOC; and (3) the element Ba, which may
345 be indicative of hydrothermal processes.

346

347 *4.4.1 Redox proxies*

348 High values of the ratios V/Al and Mo/Al are generally thought to indicate reducing conditions
349 (Tribovillard et al., 2006). V/Al curves from both the Pecos and Winkler County cores are
350 presented in Figure 7. Both data sets show relatively low values throughout most of the
351 section, typically 0.20 to 0.50, punctuated by anomalous intervals with ratios that are 2 to more
352 than 10 times background. The anomalous intervals range in thickness from 2 to 15 meters of
353 stratigraphic thickness. Based on a compacted sedimentation rate of 4 meters per million years
354 and assuming continual and steady sedimentation, the anomalies represent periods of time
355 ranging from 500,000 to almost 4 million years (Re-Os age dates are presented below).

Discontinuities in sedimentation rate could expand or contract the time interval represented by the anomalies.

Even with a sampling frequency of approximately 1 meter, V/Al anomalies can clearly be correlated between the two wells (Fig. 7), although the wells are 120 km apart. Both the curve shapes and absolute ratios are similar. Correlation of the V/Al curves is consistent with correlations based on gamma log patterns (Fig. 2), which as noted previously, largely reflect uranium content and TOC.

Mo/Al ratios are shown for the same samples in Figure 7. Ratios are typically in the range of 0.05 to 0.15, with the exception of one interval near the bottom of the sampled section in the Pecos County core. Peak ratios range from 0.25 to 0.60, so the difference between background and peak is slightly less than with the V/Al ratios. The location of high Mo/Al peaks differs almost completely from the V/Al ratios, also reflected by the different factors with which Mo and V are associated. The Mo/Al curves can also be correlated in detail between wells (Fig. 7).

The concentration of phosphate in sediments has been shown to depend on redox conditions, with phosphate effectively recycled to sea water under reducing conditions (Ingall et al., 2005). Phosphate values vary significantly throughout the core. Plotted as TOC/P_{tot} (Fig. 7), three intervals of the formation are distinguished in the core, a lower section characterized by low values, typically between 5 and 25, a middle section characterized by high values between 40 and 240, and an upper section characterized by extremely low values between 0.7 and 4. Large

phosphate nodules are evident in core in the upper section but not in the middle and lower sections. The three sections correspond only approximately to the Lower, Middle and Upper Woodford subdivisions based on gamma logs (Fig. 2-4).

4.4.2 Basin reservoir effect

The ratio of redox sensitive trace metals such as Mo to TOC has been used to indicate metal replenishment and basin restriction (Algeo and Lyons, 2006), where low values of these ratios are taken to indicate greater degrees of restriction. Median values for Mo/TOC in the Pecos County and Winkler County wells are 11.4 and 11.9 (Figure 4). An overall upward decrease is evident in the Pecos County well, but with a high degree of small-scale variability. Values in the Winkler County well are similar, although the upward decrease is not evident because the stratigraphic range of the sampled section is more restricted.

The Cu/TOC and Ni/TOC curves (Fig. 7) are grossly similar to Mo/TOC, also decreasing upward in the Pecos County well. Differences between the Mo/TOC and Cu/TOC curves exist at 3965, 3955 and 3892 meters in this well. The two deeper anomalies correspond to intervals of elevated clay content and reduced TOC/P_{tot}.

4.4.3 Barium anomalies

Barium concentrations in the two wells display a relatively constant background level, with isolated samples that spike to much higher levels (Fig. 7). In the Pecos County well, the typical value of Ba content ranges from 900 to 1800 ppm. Isolated high values range from 3000 to

17600 ppm. In the Winkler County well, both background and peak values are lower. Background values decrease from 600 in the Lower Woodford to 400 in the Upper Woodford, and peak values are from 1200 to 2550 ppm. The anomalies are dispersed continuously through the section, and the peaks do not show systematic stratigraphic variation. Ba is uncorrelated with TOC.

4.5 Re-Os Geochemistry

With the exception of the shallowest stratigraphic interval studied (3889.53 – 3889.83 m), sample sets have similar Re abundances ranging from 22 to 102 ppb, increasing slightly up section (3972.84-3973.1 m = ~22-69 ppb; 3944.14 – 3944.41 m = ~26-89 ppb; 3912.15 – 3912.38 m = ~32-102 ppb; Table 3; Fig. 8). Common Os abundances, expressed as ^{192}Os, are constant or decrease up section (3972.84-3973.1 m = ~211-614 ppt; 3944.14 – 3944.41 m = ~102-262 ppt; 3912.15 – 3912.38 m = ~58-190ppt). The shallowest sample set (3889.53 – 3889.83 m) has some individual samples with Re and ^{192}Os abundances similar to the deeper sample sets, and others that contain much higher Re and ^{192}Os values.

In all four sample sets, ^{187}Re/^{188}Os values are positively correlated with ^{187}Os/^{188}Os values (Table 3; Fig. 9). The deeper three sample sets individually possess distinct Re-Os isotope compositions, with higher ^{187}Re/^{188}Os and more radiogenic ^{187}Os/^{188}Os values up section. The shallowest sample set possesses ^{187}Re/^{188}Os and ^{187}Os/^{188}Os values similar to and greater than

421 the set from 3944.14-3944.41, but less than the set from 3912.15 – 3912.38 m (Table 3; Figure
422 9).

423 The Re–Os isotopic data, 2σ calculated uncertainties for $^{187}Re/^{188}Os$ and $^{187}Os/^{188}Os$ and the
424 associated error correlation function (rho) are regressed to yield a Re–Os date using *Isoplot V.*
425 *3.0* with a $\lambda^{187}Re$ constant of 1.666 **x** 10^{-11} a^{-1} (Ludwig, 1980, 2003; Smoliar et al., 1996; Fig.
426 10). The Re-Os data for the base of the Woodford Fm, (3972.84-3973.1 m) yield a Re-Os age of
427 379.0 ± 7.9 Ma (MSWD = 3.5; initial $^{187}Os/^{188}Os$ = 0.29 ± 0.03; middle Frasnian - Devonian; Fig.
428 10A). The lower and upper parts of the middle Woodford, (3944.14 – 3944.41 m; 3912.15 –
429 3912.38 m), yield Re-Os ages of 371.5 ± 5.8 Ma (MSWD = 0.58; initial $^{187}Os/^{188}Os$ = 0.40 ± 0.06;
430 Fig. 10B) and 364.0 ± 13 Ma (MSWD = 0.28; initial $^{187}Os/^{188}Os$ = 0.69 ± 0.25; Fig. 10C),
431 respectively (spanning the Famennian; Ogg et al., 2008). The uppermost sample set (3889.53 –
432 3889.83 m) from the upper Woodford, yields a Re-Os date of 357.9 ± 5.3 Ma (MSWD = 2.1;
433 initial $^{187}Os/^{188}Os$ = 0.47 ±0.07; Fig. 10D; Tournaisian).

434

435 **5. Discussion**

436

437 *5.1 Depositional Ages and Sedimentation Rates*

438

439 Re-Os age dates reported here provides constraints on the age of the Woodford that are
440 consistent with biostratigraphic ages reported by Comer (1991) and Meyer and Barrick (2000).
441 A radiometric date obtained from 35 meters above the base of the Woodford section in the

Pecos County well is middle Frasnian, compared to a biostratigraphic age of uppermost Givetian reported for the base of the Woodford (Comer, 1991; Meyer and Barrick, 2000). The uppermost sample obtained from one meter below the stratigraphic top of the Woodford yielded a lowermost Mississippian date, identical to reported biostratigraphic ages (Comer, 1991; Meyer and Barrick, 2000). Biostratigraphic dating was attempted on the Pecos County core, but no conodonts were recovered. Typically, relatively large amounts of sample are required for conodont dating, more than was possible given core archiving protocols.

The Woodford age dates, whether biostratigraphic or radiometric, place this formation as time-equivalent to a number of other shale formations in North America. The date of the sample from 3944 meters core depth is similar to that of the reported by Turgeon et al. (2007) for the Hanover Formation in the Appalachian Basin of western New York State. The age of the shallowest sample from 3889.53 – 3889.83 m is 357.9 ± 5.3 Ma, just younger than the Devonian – Mississippian boundary dated from the Exshaw Formation in the Western Canada Sedimentary Basin by Re-Os at 361.3 6 2.4 Ma (Selby and Creaser, 2005).

The Woodford Shale dates yield a best estimate of overall compacted sedimentation rate of 4 meters per million years in the Pecos County core. The section in the Winkler County is expanded by approximately 30%, suggesting a best estimate of 5.2 meters per million years in the basin center. These overall rates are similar to other reported rates for black shales. Maynard (1980) in his compilation of sedimentation rates in Mississippian and Devonian shales recorded sedimentation rates ranging from 1 to 60 meters per million years. Lazar (2007)

estimated rates of 1 to 7 meters / Myr for different systems tracts of the New Albany Shale (Upper Devonian, Illinois Basin).

5.2 Trace Element Enrichment

While organic-rich mudstones are commonly thought to be enriched in metals relative to average shale, many trace metals in the Woodford Shale are at average shale levels or are depleted (Fig. 6). Only Mo, U, S and Se are highly enriched. Cd, Ni, Ag, As, Sb, Ba and Hg show moderate enrichment in many but not all samples. Metals that are not enriched include Pb, Bi, Cr, Tl (all depleted), Co, Zn, Cu and V (approximately average). This result contrasts with studies of many organic-rich mudstones. Lipinski et al. (2003), for example, described enrichment in Co, Cr, Cu, Tl and Zn in Jurassic and Cretaceous shales from the Norwegian Shelf. Lipinski et al. (2003), citing data in Arthur et al. (1990) and Warning and Brumsack (2000), noted that Cenomanian-Turonian black shales are enriched in Bi (average 2.3 X average shale), Co (1.7X), Cr (1.52X), Cu (4.18X), Tl (5.15X), V (5.68X) and Zn (12.77). That the Woodford displays such different patterns in metal enrichment suggests that the Devonian organic-rich shales may have had a significantly different origin from the younger black shale formations, either because of basin configuration (reservoir effect; see below) or because of different global ocean chemistry.

Two mechanisms may have played a minor role in the lack of significant enrichment of trace metals. First, some metals, Ni and V in particular, are known to fractionate into oil phases (Lewan and Maynard, 1982; Branthaver and Filby, 1987). The relatively depleted metal

concentrations may therefore be a function of oil generation and expulsion. Because the Woodford section in the Pecos County well is more deeply buried than in the Winkler County well and has generated significant amounts of oil, based on the higher thermal maturity, it would be expected that Woodford section here should have lower metal contents if this has a significant effect. A comparison of five elements shows a systematic depletion averaging approximately 15% in Pecos County well relative to the Winkler County well, suggesting that oil generation and expulsion may have had a relatively minor effect.

Second, dilution, for example by carbonate minerals or quartz, may have also reduced trace element concentrations. In the Woodford Shale, the primary diluting mineral is quartz, which we have elsewhere interpreted as largely biogenic in origin (Harris et al., 2009; Hemmesch et al., in press). This effect can be tested by comparing raw enrichment factors ($Me_x/Me_{avg\ shale}$) to enrichment factors that are normalized to aluminum, which eliminates the effect of dilution. A comparison of raw enrichment factors to a aluminum-normal enrichment factors (Table 1) therefore measures the effect of dilution. The aluminum-normalized median trace metal enrichment factor scores average 19% higher than the raw enrichment factors, with Cu, Zn and V concentrations increasing from approximately similar to average shale values to slightly enriched. These effects indicate that dilution played a measureable but relatively minor role in decreasing trace metal concentrations. Moreover, aluminum concentrations are higher in the KCC well than in RTC well, probably a function of proximity to the northern basin margin with exposed siliciclastic terrane; thus the modestly lower trace element concentrations in the KCC well are probably a result of greater dilution, not an association with expelled hydrocarbons.

508

509 *5.3 Trace Element Associations*

510

511 Factor analysis identified a number of trace and minor element associations (Table 1). Two
512 factors clearly represent suites of minerals and are associated with distinct types of sediment
513 sources. Factor 1 is related to detrital clays or feldspar, based on the Al_2O_3, K_2O and Na_2O
514 contents; trace elements associated with Factor 1 are TiO_2 and elements typically found in
515 granitic crust: Cs, Ga, Hf, Nb, Rb, Th and Bi. Factor 4 includes carbonate-related elements and
516 SiO_2; MnO, whose concentration is generally low, is positively correlated with this factor,
517 indicating that its concentration is primarily related to carbonate content.

518

519 Other factors represent controls by water column and sediment chemistry. The strong
520 association in Factor 3, between TOC, U, and Mo (Table 1; Fig. 11A, B) is clearly a redox control;
521 these elements are concentrated under anoxic conditions, and strong relationships with TOC
522 have been described by many authors. Fe and S are very highly correlated with Factor 6. This
523 indicates that (1) Fe is effectively completely scavenged by sulfide, which must have existed in
524 excess of Fe in the water column; and (2) that sulfidation of iron (Factor 6) was decoupled from
525 other redox proxies (Factor 3), similar to observations from Recent Black Sea sediments (Lyons
526 and Berner, 1992).

527

528 Other aspects of trace and minor element concentrations are problematic, however:

529

1) V, a redox-sensitive element whose behavior typically parallels U and Mo, is neither enriched (Fig. 6) nor correlated with TOC, U and Mo (Table 1; Fig. 11a, b).

2) Cr, considered to be a redox-sensitive element, is depleted and is strongly associated with the clastic fraction (Factor 1).

3) Cu and Co, whose transfers to sediment are generally thought to be related to organic matter deposition, are neither enriched nor associated with TOC content; while Ni, whose concentration is similarly controlled, is moderately enriched and is associated with TOC. Ni and Cu are poorly correlated (Fig. 11D), which is unusual in black shales.

4) While phosphate concentrations are generally low, in the lower and particularly in the upper part of the Upper Woodford, phosphate concentrations increase significantly despite locally high TOC contents and abundant pyrite (Fig. 7). Phosphate is not associated with Mo or U, appearing in a separate factor (Factor 7) and is uncorrelated with the redox proxy Mo/Al_2O_3 (Fig. 11C).

Tribovillard et al. (2006) described sources of complexity in the application of trace metals: different redox thresholds; different mechanisms by which elements are sequestered in the sediment; differing reaction rates; and biogenic pathways for remobilizing elements in the water column and the sediment. Another complication is the 'basin reservoir effect', described by Algeo and Lyons (2006), in which chemical components are transferred from an isolated

552 deep water mass to the sediment faster than the rate at which these components are renewed
553 in the water column; as a result, concentrations of the component in the water column and
554 ultimately the sediment decrease. This phenomenon may occur with redox-sensitive elements,
555 resulting in low concentrations in the sediment even at reduced oxygen levels. Algeo and Lyons
556 (2006) applied this concept with Mo, normalized to TOC, to characterize restriction in modern
557 basins and the Devonian Appalachian shale basin (Algeo et al., 2007).
558
559 We begin by considering phosphate, which is commonly depleted in the Woodford; half of the
560 samples show concentrations from 0.07 to 1.00 times average shale values. Depletion is
561 common in organic-rich shales because reducing conditions in the sediment allow phosphate to
562 dissolve into pore water and diffuse from the sediment. Depletion in phosphate is particularly
563 strong when considered in relationship to TOC; ratio of TOC/P_{tot} in the Woodford averages 647
564 and 445 in the Winkler and Pecos County wells, similar to or higher than many ancient black
565 shales (Algeo and Ingall, 2007), which indicates that the sediment pore waters were strongly
566 reducing. The generally low P_2O_5 is consistent with the strong correlation between Fe and S.
567 Various authors (Benitez-Nelson, 2000; Tribovillard et al., 2006) have noted that Fe-
568 oxyhydroxides and clays play a role in the precipitation of remineralized phosphate; but where
569 Fe is effectively scavenged by H_2S, no Fe-oxyhydroxides are available.
570
571 V behaves differently from other redox proxies such as U and Mo in our data set (Figures 7,
572 11A, B), much less enriched and associated with a different factor (Factor 5). The Holocene
573 section in the Orca sub-basin, Gulf of Mexico (Tribovillard et al., 2008) may be an instructive

analog; elevated Mo values reflect anoxic conditions, but unusually low U, V and Cu are attributed to the basin reservoir effect (see below). A similar mechanism may have functioned in the Woodford.

Decoupling of V from U and Mo may also have been related to another factor. Vanadate is deposited through adsorption onto Mn- and Fe-oxyhydroxides in the water column (Tribovillard et al., 2006). In the Woodford Shale, Mn values are low and strongly tied to carbonate minerals, suggesting that Mn-oxyhydroxides were absent or limited. Fe and S are tightly coupled, indicating that all iron was sequestered at the time of deposition in sulfides and therefore unavailable as oxyhydroxides. The lack of V enrichment as well as depleted Zn, Pb and Co may therefore be related to the absence of a substrate in the water column on which to precipitate.

5.4 Stratigraphic Variability, Redox Conditions, and Basin Reservoir Effect

Redox conditions in a sedimentary basin are the complex function of biochemical and physical oceanographic processes. Oxygen is mixed into the water column at the water surface through wave action and diffusion. Oxygen is also added to the water column by exchange with oxygen-rich water bodies from the open ocean, and as exchange increases, oxygen levels rise. Oxygen levels decrease largely through consumption during oxidation of organic matter; thus at higher levels of organic productivity, more oxygen is consumed. Organic production is largely related to nutrient supply, which may be delivered from the open ocean, usually in locations of deep water upwelling but sometimes also associated with major river systems.

596

597 The effects of sea level change on redox conditions can be complex, particularly where the
598 bathymetry of a basin creates partial barriers between it and the open ocean. Falling sea level,
599 for example, could decrease mixing with oxygenated open marine water, but oxygen from
600 surface waters could be mixed to a relatively greater depth; moreover, if nutrient flux from the
601 global ocean decreases as a result of greater restriction, then organic productivity would
602 decrease, which in turn would decrease oxygen demand within the water column. Conversely,
603 rising sea level could increase mixing of oxygenated ocean water but might at the same time
604 increase nutrient delivery, organic productivity and oxygen demand.

605

606 While Mo and U show a strong relationship to TOC, as described above, the ratios of Mo to TOC
607 are lower than expected for basins with rapid exchange with the global ocean. This is the 'basin
608 reservoir effect', and median values for Mo/TOC in the Pecos County and Winkler County wells
609 are 11.4 and 11.9, respectively, well within the range for 'strong restriction' described by Algeo
610 and Lyons (2006) that indicates limited Mo renewal. The upward decrease in Mo/TOC in Pecos
611 County well (Fig. 7) suggests increasing restriction, consistent with an overall fall in relative sea
612 level documented on the basis of sedimentological and stratigraphic data (Hemmesch et al., in
613 press). Fluctuations around the overall decrease probably reflect the effect of 3rd order sea
614 level cycles, superimposed on a 2nd order sea level fall. Paleogeographic reconstructions
615 (Section 2), however, provide only limited confirmation that the Late Devonian Permian Basin
616 was restricted. Barriers to circulation existed to the east and west of the basin, the Concho

Arch and Diablo Platforms, respectively (Fig. 1C). But the nature of the southern connection to the Rheic Ocean was obscured by post-Devonian tectonic events.

The Winkler County well does not show a similar decline in Mo/TOC. However, it should be remembered that although this and the Pecos Country cores are similar in length, the Winkler Country core represents a much smaller part of the Woodford section because of expansion of the section closer to the northern margin of the basin.

We may test whether other trace metals are subjected to the basin reservoir effect by comparing the metal (Me)/TOC curves to Mo/TOC. Cu is of particular interest because it is depleted in comparison to Ni (Fig. 10D). The Cu/TOC and Mo/TOC curves are grossly similar, with both curves generally decreasing upward (Figure 7); this suggests that Cu deposition, like Mo, drew on a limited supply of that element from a partially isolated body of deepwater. In detail, Cu/TOC largely matches Mo/TOC, but differences exist at 3965, 3955 and 3892 meters. The two deeper anomalies correspond to intervals of elevated clay content and reduced TOC/P, suggesting increased oxygen levels during deposition of these intervals; the presence of elevated Cu/TOC and Ni/TOC suggests increased nutrient delivery may have been high, with Cu and Ni fixed in sediments, but that the organic matter itself largely decomposed in the sediment under enhanced oxygen levels.

The TOC/P_{tot} data display two distinct stratigraphic transitions, from relatively low values in the Lower Woodford to high values in the Middle Woodford to very low values in the Upper

639 Woodford; this pattern suggests that redox conditions in the Permian Basin water column
640 periodically underwent abrupt changes. In the Upper Woodford, development of low TOC/P_{tot}
641 and the presence of phosphate nodules imply that a redox front existed within the sediments
642 and that elevated oxygen levels were present in the water column. We identify two possible
643 drivers for the increased oxygen levels: (1) decreased water depths during a 2nd or 3rd order sea
644 level fall allowed more complete mixing of oxygen through the water column, or (2) a rise in
645 atmospheric oxygen (Algeo and Ingall, 2007) charged surface waters with higher levels of
646 dissolved oxygen.
647
648 Despite much lower TOC/P_{tot} values in the upper 8 meters of sampled Pecos County section
649 that indicate an increase in oxygen levels, Mo/ Al_2O_3 ratios here are relatively high, which
650 suggests reducing conditions. We suggest that the contrasting behavior of redox-sensitive
651 elements may have resulted from different kinetics in precipitation mechanisms. Fixation of
652 trace metals in sediment is significantly faster than the fixation of phosphate (Algeo and Ingall,
653 2007); possibly the sediment records short-term anoxic events in the metals that resulted in Mo
654 precipitation, while at the same time recording a longer-term increase in oxygen levels in the
655 phosphate. This model requires that kinetics of metal precipitation be faster than dissolution.
656
657 The lower transition from low to high TOC/P_{tot} is very close to the Re-Os sample that yielded a
658 date of 371.5 ± 5.8 Ma, and we suggest that the transition is related to the Frasnian –
659 Famennian boundary event (the boundary itself is dated by Turgeon et al. (2007) using Re-Os at
660 372.4±3.8 Ma). In our data, the shift to high TOC/P_{tot} is accompanied by a one sample decrease

661 in Mo/TOC to low value (Fig. 7); this suggests that (1) the change in redox conditions was
662 induced by a significant but short-lived fall in sea level, and (2) the subsequent rise in sea level
663 did not return redox conditions to their previous state. In the Woodford data, the transition is
664 not marked by a notable change in the organic carbon content (Fig. 7).
665
666 According to some authors, the Frasnian – Famennian boundary event was marked by a sharp
667 drop in sea level (Haq and Schutter, 2008; Chen and Tucker, 2004), although this view is not
668 universally held (cf. Bond and Wignall, 2008). Such a model is consistent with our data,
669 although we lack the age control that other studies have (e.g. Chen and Tucker, 2004; Bond and
670 Wignall, 2008). Assuming, however, that the sharp transition in TOC/P_{tot} equates
671 approximately to the Frasnian – Famennian event, there is no increase in organic carbon
672 deposition that would suggest unusual segregation of carbon in the form of deposited reduced
673 carbon; rather the entire section is enriched in organic carbon.
674
675 A similar but even sharper decrease in Mo/TOC occurs at 3965.0 meters, a short distance below
676 the one that we tentatively associate with the F/F event. In this case, Mo/TOC decreases from
677 12.9 to 0.901 (ppm/%), before rebounding to 6.89 and 7.48 in the two overlying samples.
678 TOC/P_{tot} increases in this and the two samples above, suggesting development of more
679 reducing conditions, albeit at a much lesser scale and for a less extended period of time than in
680 the major event above.
681

682 The Mo/Al curve (Fig. 7), a common redox proxy, only partially tracks the TOC/P_{tot} curve. One
683 interval in which the curves behave in parallel is the section containing what we infer to be the
684 Frasnian-Famennian boundary. In the samples showing a sharp rise in TOC/P_{tot}, the Mo/Alcurve
685 increases from 4.68 to 25.81. The 'saddle' (high-low-high) in the TOC/P_{tot} curve between
686 3914.24 and 3947.16 meters is largely paralleled by the Mo/Al curve. But at other points, the
687 curves behave differently. The maximum in the Mo/Al curve at 3906.92 m is not matched in
688 the TOC/P curve.
689
690 Barium concentration has been identified as a productivity proxy, but it is also sensitive to
691 water depth (Dymond et al., 1992; Hernandez-Sanchez et al., 2011); moreover, its application
692 as a productivity proxy is suspect in settings where sulfate is reduced to sulfide (Dymond, 1992)
693 as is presumably the case here. Barium values are typically moderate in the Woodford
694 sediments, with local spikes to much higher values, particularly in the Pecos Co. well in which
695 Ba peaks are almost an order of magnitude higher than in the Winkler Co. well (Figure 7).
696 Background Ba values also differ between the two wells, lower by a factor of two in the Winkler
697 County well in the basin center. If background Ba values do reflect paleoproductivity, then
698 paleoproductivity was higher near the western margin of the basin, perhaps due to upwelling,
699 but there is no corroborating evidence for such an interpretation.
700
701 We suggest two possible alternative mechanisms for locally high Ba values. First they may
702 represent syndepositional hydrothermal events. If this model is correct, this would suggest that
703 Ba was probably sourced from the western margin of the basin and that Ba concentrations

704 decreased away from the source. In addition, Ba anomalies cannot be correlated between the
705 wells, suggesting that such events were relatively localized.
706
707 Our preferred explanation is that anomalous Ba concentrations represent a preserved chemical
708 front, the sulfate-methane transition, above which Ba is insoluble due to the presence of excess
709 sulfate but below which Ba is soluble because sulfate is absent (Henkel et al., 2012). Ba
710 anomalies are preserved in the sediment record during times of low sedimentation, increased
711 sulfate concentrations or low methane generation. We see no obvious indication in other
712 geochemical data of decreased methanogenesis or sulfate penetration; but periods of low
713 sedimentation are entirely plausible, given our interpretations of approximately 10 third order
714 sea level cycles (Hemmesch et al., in press). In this case, we suggest that each enriched horizon
715 marks a maximum flooding surface, although the horizon at which the Ba anomaly occurs
716 should not represent the time of slow sedimentation; instead, the maximum flooding surface is
717 some distance above the Ba anomaly. Moreover, the fact that the anomalies are much
718 stronger in the Pecos Co. well suggests that depositional rates were lower and sedimentary
719 hiatuses were more pronounced here than in the Winkler Co. well, consistent with the
720 expanded Woodford section in the Winkler Co. well.
721
722 *5.5 Re-Os Geochemistry*
723
724 *5.5.1 North American Frasnian-Famennian seawater Os isotope composition*

725 The Re-Os samples span almost the complete Woodford section, including the Frasnian –
726 Famennian and Devonian – Mississippian boundaries. As noted above and described in detail in
727 Hemmesch et al. (in press), the section is characterized by a relative second order sea level fall
728 with superimposed third order sea level cycles. The second order sea level fall resulted in
729 increased restriction of the basin from the global ocean, demonstrated by decreasing ratios of
730 some redox-sensitive metals to TOC: Mo/TOC, Cu/TOC and Ni/TOC. Redox proxies indicate
731 overall low levels of oxygen in the water column during this time, but distinct changes in redox
732 conditions occurred, marked by variations in trace metal and TOC/P_{tot} ratios.
733
734 The initial $^{187}Os/^{188}Os$ (Os_i) value of organic-rich sedimentary units is used to evaluate the
735 $^{187}Os/^{188}Os$ value of the water column at the time of deposition (cf. Cohen, 2004 and references
736 therein). Although the Woodford shale records a sea level fall up section and the trace element
737 data are interpreted to reflect increasing basin restriction, the Os_i data (Table 3) suggest that
738 either (1) the Permian Basin remained interconnected with the other North American and
739 European basins (e.g., Peace River, Appalachian, Rhenohercynian Basins; Fig. 1) or (2) the
740 isotopic composition of Os entering the individual basins, derived from the weathered
741 continental mass, was extremely similar. For example, the inferred Frasnian – Famennian
742 boundary interval of the Pecos County well possesses an Os_i value of 0.40 ± 0.06 (Table 3; Fig.
743 10B), which is, within uncertainty, identical to the age-equivalent interval of the Hanover
744 Formation of the Appalachian Basin (WVC785 = 0.47 ± 0.04 determined from a Re-Os isochron
745 and 0.47 ± 0.02 calculated from the Re-Os data at 374 Ma; Turgeon et al., 2007). The lowermost
746 Mississippian section of the Pecos County well has an Os_i value of 0.47 ± 0.07, which is not only

very similar to the Devonian-Mississippian boundary interval of the Exshaw Formation of the Peace River Basin (0.42 ± 0.01; Selby and Creaser, 2005), but also to the upper most Devonian *praesulcata* and *Cymaclymenia nigra* Zones of the Hangenberg Shale, Germany, of the Rhenohercynian Basin (0.42 ± 0.01; 1 SD, n = 3; Table 3). In contrast, the uppermost Famennian dated interval of the Permian basin (Pecos County well, 3912.15 – 3912.38 m) possesses a more radiogenic Os_i value (0.69 ± 0.25) than that of a time-equivalent interval of the Appalachian Basin (0.45 ± 0.02 from section WVC754; Turgeon et al., 2007). Given that the residence time of Os in the ocean is between ~10 to 40 Kyr (Peucker-Ehrenbrink and Ravizza, 2000), the difference in the Os_i values between the upper Famennian intervals of the Permian and Appalachian Basins may be because they are from slightly different stratigraphic horizons or because the Os isotope seawater composition in the individual basins differed during this time period. The latter is possible given the proximity of the middle Proterozoic, isotopically-evolved, Laurentian Craton to the Permian Basin versus the Phanerozoic, less isotopically-evolved Appalachian Mountain Belt that contributed detritus to the Appalachian Basin. Lastly, the basal section of the Woodford Formation (Re-Os date = 379 ± 7.1 Ma; Fig. 10a) from the Permian Basin possesses an unradiogenic Os_i value of 0.29 ± 0.03. This section can be broadly correlated with the WVC802 section of the Hanover Formation of the Appalachian Basin, based on an age of ~378 Ma in the WVC802 section extrapolated from shallower radiometric ages (Turgeon et al., 2007). The age of 378 Ma is in agreement, within uncertainty, with the WVC802 biostratigraphic constraints (*linguiformis* biozone; Ogg et al., 2008). Using 378 Ma, the Re-Os data of the WVC802 section yield an Os_i value of 0.27 ± 0.03, very similar to the correlative interval in the Pecos County well. Nominally older, the Keg River Laminite, Upper Member

769 laminites, La Crete Basin, Canada possess an Os_i value of 0.26 ± 0.03 determined from Re-Os
770 geochronology (382.2 ± 6.9 Ma; MSWD = 2.5; Miller, 2004). Nominally younger, the mid-Frasian
771 Duvernay Formation, West Shale Basin, Alberta, Canada (~378 Ma; McLean and Klapper, 1998)
772 possesses Os_i values of 0.35 ± 0.01 (1 SD, n = 3; Table 3). Although the Canadian (Keg River and
773 Duvernay Formations) and USA (Hanover Formation) sections are broadly correlated to the
774 Peco County Core at ~379 Ma, the sections all possess very similar unradiogenic Os_i,values
775 suggesting that the Givetian and Frasian ocean was characterized by an unradiogenic Os
776 isotope composition that was either controlled by a reduced rate of continental weathering or
777 that continental weathering was predominantly controlled by an unradiogenic source.
778
779 Thus, with the exception of the uppermost Famennian interval of the Permian Basin (0.69 ±
780 0.25; Fig. 10c), the Os_i values of the Woodford Formation are very similar to those of correlated
781 areas of the Hanover, Exshaw and Hangenberg Black Shale Formations of the Appalachian, La
782 Crete, West Shale, Peace River and Rhenohercynian Basins, respectively. This similarity implies
783 that the basins were hydrologically connected or that the input in to the individual basins was
784 extremely similar in Os isotope composition.
785
786 *5.5.2 Re and Os enrichment and Fractionation in Organic-rich Sedimentary rocks*
787 The Re-Os data for the three stratigraphically older sample sets show with decreasing age a
788 subtle increase in Re (average values = ~44 ± 17 to 74 ± 31 ppb) and a decrease in common Os
789 (^{192}Os; average values = ~340 ± 138 to 160 ± 131 ppt; Fig. 8). This trend coincides with
790 development of an anoxic water column, indicated by increased TOC/P_{tot}. The stratigraphically

youngest sample set shows much higher in Re abundances (>110 to ~466 ppb), similar to distinctly higher ^{192}Os values (241 to 1064 ppt; Figure 8). TOC/P_{tot} in this sample reverts to very low values, indicating a more oxygenated water column.

The stratigraphically youngest Re-Os sample set comes from a section of lower average TOC in which the organic matter contains a much greater terrestrial component than most of the formation (Fig. 4). These observations, together with lower TOC/$P_{tot,}$ suggest a more oxidizing water column for the lowermost Mississippian Woodford Formation.

Low levels of oxygen in the water column are considered to be a key factor in controlling the uptake of Re and Os in organic-rich sedimentary rocks, where highly reducing conditions favor the enrichment of Re over Os (e.g., Morford and Emerson, 1999 and references therein; Peuker-Ehrenbrink and Ravizza, 2000; Yamashita et al., 2007; Georgiev et al., 2011 and references therein). This would predict that the lowermost Mississippian horizon of this study should therefore possess the least Re and Os enrichment of the sampled Woodford Formation intervals. However, our Re-Os data show that the organic-rich sediments of the Woodford Formation deposited in the most oxygen-enriched water column possess the highest Re and Os abundances, and have the most variable and some of the highest ^{187}Re/^{188}Os values (Table 3; Fig. 10). These observations are inconsistent with a strong positive relationship between the water column redox condition and Re-Os systematics (Selby et al., 2009).

In addition to differences in oxygen levels in the water column associated with the middle and upper Woodford Formation, other characteristic differences between the middle and upper Woodford intervals are TOC abundance and organic matter type. The kerogen component of organic matter is the principal host to Re and Os in organic-rich sedimentary rocks (Rooney et al. 2012). Given that TOC levels in our Re-Os samples were similar and that organic matter only provides a fundamental binding site for Re and Os (Rooney et al., 2012), the TOC content cannot be considered a controlling factor of Re and Os enrichment (Cohen et al., 1999; Selby et al., 2009). However, the sample set from the Lower Mississippian interval contains a mixture of terrestrial and marine-derived organic matter, whereas the three sample sets from the upper Devonian section contain only amorphous marine-derived organic matter (Fig. 3). The mix of organic matter types thus may be the controlling factor on Re and Os enrichment in organic-rich sedimentary rocks and any variation in $^{187}Re/^{188}Os$ values. Cumming et al. (2012) reached a similar conclusion based on Re-Os data from the Green River Formation.

Other potential controls for Re and Os enrichment in organic-rich sedimentary rocks may relate to Re and Os abundance in the water column (Turgeon et al., 2007), sedimentation rate (Lewan and Maynard, 1982; Crusius and Thomson, 2000), salinity, pH, temperature (Martin et al., 2001; Georgiev et al., 2011), and post-depositional mobility (Crusius and Thomson, 2000; Kendall et al., 2009). The lowermost Mississippian interval represents the period of greatest restricted ocean circulation during deposition of the Woodford Shale in the Permian Basin, based on Mo/TOC ratios (Fig. 7), which would normally imply similar to less enrichment of Re and Os as compared to the Devonian Woodford Sections. The fact that the lowermost Mississippian

834 interval is more enriched in Re and Os (Fig. 8) suggests that Re and Os were either more
835 enriched in the Lower Mississippian Permian Basin seawater and / or an alternate enrichment
836 mechanism existed. Moreover the Woodford shows no evidence for changes in sedimentation
837 rate, salinity, pH and temperature of the water column; and post-depositional mobility of Re
838 and Os are not indicated, given the isochronous behavior of the Re-Os isotope systematics. As a
839 result, we propose that variable organic matter type may, at least in part, control Re and Os
840 enrichment and thus Re-Os fractionation in organic-rich sedimentary rocks.
841
842 **6. Conclusions**
843
844 Our examination of trace and minor element concentrations in the Woodford Shale highlights
845 both similarities and differences between this and other organic-rich shales. The Woodford is
846 enriched in some trace metals, similar to other black shales, notably Mo, U, and S and to a
847 lesser extend Cd, Ni and Ba, but it is not enriched – even depleted – in others such as Pb, Cr, Co,
848 Zn, Cu and V.
849
850 The trace metal data demonstrate a strong basin reservoir effect, evident in ratios of Mo, Cu
851 and Ni to TOC. Mo/TOC ratios at the base of the Woodford section are lower than predicted for
852 a basin with unrestricted exchange with the open ocean; these ratios decrease upward, the
853 effect of decreasing sea level. Thus even while Mo is relatively enriched, a redox effect, the
854 enrichment is less than would have been the case in an unrestricted basin.
855

856 Depletion in other metals such as Cr, Co, Zn and Cu probably has a number of causes, including
857 the basin reservoir effect, dilution by biogenic silica and possibly mobilization into an expelled
858 hydrocarbon phase.
859
860 The data also demonstrate complexities in the interpretation of redox proxies. Uranium and
861 Mo proxies behave coherently; V, generally thought to vary in parallel with these proxies,
862 behaves very different, displaying peaks and troughs at very different stratigraphic points.
863 These suggest different precipitation mechanisms for the metals.
864
865 We tentatively identify the Frasnian – Famennian boundary event, based on a striking increase
866 in the ratio TOC/P_{tot}, indicating the development of strong water column anoxia. The transition
867 to high TOC/P_{tot} is associated with pronounced but short-lived decrease in sea level, based on
868 Mo/TOC ratios. Although sea level appeared to have rebounded after this event, the
869 development of an anoxic water column was apparently quite stable, persisting until quite late
870 in Woodford deposition when sea level had reached a much lower level.
871
872 Re-Os analysis provides constraints on depositional ages and basin hydrology during Woodford
873 deposition. Ages range from middle Frasnian at the base of the sampled section to lowermost
874 Tournaisian at the top, confirming published biostratigraphic ages. Os_i values in most of the
875 section are similar to published values from coeval sections in the Peace River Basin in Canada,
876 the Appalachian Basin in the eastern United States, and the Rhenohercynian Basin in Europe.
877 This is interpreted to indicate that the Devonian basins, even when the sea level was low and

878 the basins were restricted, remained connected to global ocean water. Our uppermost
879 Famennian sample differs considerably from a coeval Appalachian Basin sample, possibly due to
880 contributions on less radiogenic Os from Phanerozoic sources into that basin. Finally,
881 enrichment in Re and Os and fractionation in the shallowest sample is attributed to a control by
882 organic matter type, preferentially deposited in association with terrestrial organic matter.
883
884
885 **Acknowledgements**
886
887 We thank colleagues and friends who have contributed significantly to this work, especially
888 Nikki T. Hemmesch and Sheven Poole. Pioneer Natural Resources and Whiting Petroleum Co.
889 contributed cores to this study. Reviews by Thomas Algeo and an anonymous reviewer were
890 extremely constructive and helpful, and we are grateful to them. We also thank Chemical
891 Geology editor Dr. Uwe Brand for his thorough and efficient handling of our manuscript.
892 Finally, we acknowledge members of the Colorado School of Mines Woodford Shale
893 Consortium who funded the research: ConocoPhillips, Devon, Encana, EOG Resources, Newfield
894 Exploration, Petro-Hunt, Pioneer Natural Resources, and Whiting Petroleum.
895
896 **References**
897
898 Acme Analytical Laboratories, 2013. http://acmelab.com/pdfs/Acme_Price_Brochure.pdf,
899 downloaded July 18, 2013.

900 Algeo, T.J., Ingall, E., 2007. Sedimentary C_{org}:P ratios, paleocean ventilation, and Phanerozoic
901 atmospheric pO_2. Palaeogeog. Palaeoclimatol. Palaeoecol. 256, 130-155.
902
903 Algeo, T.J., Lyons, T.W., 2006. Mo-total organic carbon covariation in modern anoxic marine
904 environments: Implications for analysis of paleoredox and paleohydrographic conditions:
905 Paleoceanography, 21, 23 pp.
906
907 Algeo, T.J., Lyons, T.W., Blakey, R.C., Over, D.J., 2007. Hydrographic conditions of the Devono-
908 Carboniferous North American Seaway inferred from sedimentary Mo-TOC relationships.
909 Palaeogeog. Palaeoclimatol. Palaeoecol. 256, 204-230.
910
911 Arthur, M.A., Brumsack, H.-J., Jenkyns, H.C., Schlanger, S.O.,1990. Stratigraphy, geochemistry ,
912 and paleoceanography of organic carbon-rich Cretaceous sequences, in Ginsburg, R.N.,
913 Beaugoin, B. (Eds.), Cretaceous Resources, Events and rhythms. Elsevier, Amsterdam, p. 75-119.
914
915 Benitez-Nelson, C.R., 2000. The biogeochemical cycling of phosphorus in marine systems. Earth-
916 Science Reviews. 51, 109–135.
917
918 Bond, D.P.G., Wignall, P.B., 2008. The role of sea-level change and marine anoxia in the
919 Frasnian-Famennian (Late Devonian) mass extinction. Palaeogeog. Palaeoclimatol. Palaeoecol.
920 263, 107-118.
921

922 Branthaver, J.F., Filby, R.H., 1987, Chapter 5. Application of metal complexes in petroleum to
923 exploration geochemistry in Filby, R., et al. (Eds.), Metal Complexes in Fossil Fuels, ACS
924 Symposium Series, American Chemical Society, pp. 84-99.
925
926 Chen, D., Tucker, M.E., 2004. Palaeokarst and its implication for the extinction event at the
927 Frasnian – Famennian boundary. Journal of the Geol. Soc. Lond. 161, 895-898.
928
929 Cohen, A. S., 2004. The rhenium-osmium isotope system: applications to geochronological and
930 palaeoenvironmental problems. Journal of the Geol. Soc. Lond. 161, 729-734.
931
932 Cohen, A. S., Coe, A. L., Barlett, J. M., Hawkesworth, C. J., 1999. Precise Re-Os ages of organic-
933 rich mudrocks and the Os isotope composition of Jurassic seawater. Earth Planet. Sci. Lett. 167,
934 159-173.
935
936 Comer, J.B., 1991. Stratigraphic analysis of the Upper Devonian Woodford Formation, Permian
937 Basin, West Texas and southeastern New Mexico. Bureau of Economic Geology, Report of
938 Investigation 201.
939
940 Crusius, J., Thomson, J., 2000. Comparative behavior of authigenic Re, U, and Mo during
941 reoxidation and subsequent long-term burial in marine sediments. Geochim. Cosmochim. Acta
942 64, 2233-2242.
943

Cumming, V.M., Selby, D., Lillis, P., 2012. GRe-Os geochronology of the lacustrine Green River Formation: Insights into direct depositional dating of lacustrine successions, Re-Os systematics and paleocontinental weathering. Earth Planet. Sci. Lett. 359, 194-205. DOI: 10.1016/j.epsl.2012.10.012.

Dymond, J., Suess, E., Lyle, M., 1992, Barium in deep-sea sediment: A geochemical proxy for paleoproductivity: Paleoceanography, 7, p. 163-181.

Ellison, S.P., Jr., 1950. Subsurface Woodford black shale, west Texas and southeast New Mexico. Bureau of Economic Geology, Report of Investigations 7.

Georgiev, S., Stein, H.J., Hannah, J.L., Bingen, B., Weiss, H.M., Piasecki, S., 2011. Hot acidic Late Permian seas stifle life in record time. Earth Planet. Sci. Lett. 310, 389-400.

Hallam, A., Wignall, P.B., 1997. Mass Extinctions and Their Aftermath. Oxford University Press, New York.

Haq, B.U., Schutter, S.R., 2008. A chronology of Paleozoic sea-level changes. Science. 322, no. 5898, 64-68.

964 Harris, N.B., Hemmesch, N.T., Mnich, C.A., Aoudia, K., Miskimins, J., 2009. An integrated
965 geological and petrophysical study of a shale gas play: Woodford Shale, Permian Basin, west
966 Texas: Gulf Coast Associations of Geological Societies, Transactions. 59, 337-346.
967
968 Hemmesch, N.T., Harris, N.B., Mnich, C.A., Selby, D., in press, A sequence stratigraphic
969 framework for the Upper Devonian Woodford Shale, Permian Basin, west Texas: AAPG Bull.
970
971 Henkel, S., Mogollón, , J.M., Nöthen, K., Franke, C., Bogus, K., Robin, E., Bahr, A., Blumenberg, M.,
972 Pape, T., Seifert, R., März, C., de Lange, G.J., Kasten, S., 2012, Diagenetic barium cycling in Black
973 Sea sediments – A case study for anoxic marine environments: Geochimica et Cosmochimica
974 Acta., v. 88., p., 88-105.
975
976 Hernandez-Sanchez, M.T., Mills, R.A., Planquette, H., Pancost, R.D., Hepburn, L., Salter, I.,
977 FitzGeorge-Balfour, T., 2011. Quantifying export production in the Southern Ocean:
978 Implications for the Ba_{xs} proxy. Paleoceanography, 26, PA4222, doi:10.1029/2010PA002111.
979
980 Howarth, R. J., Sinding-Larsen, R. 1983. Multivariate Analysis, *in* Howarth, R. J. (ed.) Handbook
981 of Exploration Geochemistry: Statistics and Data Analysis in Geochemical Prospecting, v. 2, p.
982 207-289.
983
984 Ingall, E., Kolowith, L., Lyons, T., Hurtgen, M., 2005. Sediment carbon, nitrogen and phosphorus
985 cycling in an anoxic fjord, Effingham Inlet, British Columbia. Am. J. Sci. 305, 240–258.

Jarvie, D.M., Claxton, B., Henk, B., Breyer, J., 2001. Oil and shale gas from the Barnett Shale, Ft. Worth Basin, Texas: (abs) AAPG National Convention, June 3-6, Denver, Colorado.

Jarvie, D.M., Hill, R.J., Pollastro, R.M., 2005. Assessment of the gas potential and yields from shales: the Barnett Shale model, *in* Cardott, B. J., (ed.) Unconventional energy resources in the southern Midcontinent, 2004 symposium, Oklahoma Geol. Surv. Circ. 110, 37-50.

Johnson, J.G., Klapper, G., Sandberg, C.A., 1985. Devonian eustatic fluctuations in Euramerica. Geol. Soc. Amer. Bull., 96, 567-587.

Kendall, B., Creaser, R.A., Selby, D., 2009. ^{187}Re-^{187}Os geochronology of Precambrian organic-rich sedimentary rocks. Spec. Publ.- Geol. Soc. Lond., vol. 326, pp. 85-107.

Klemme, H.D., Ulmishek, G.F., 1991. Effective petroleum source rocks of the world: Stratigraphic distribution and controlling depositional factors. AAPG Bull. 75, 1809-1851.

Lazar, O.R., 2007, Redefinition of the New Albany Shale of the Illinois Basin: An integrated stratigraphic, sedimentologic, and geochemical study. Ph.D. dissertation, University of Indiana, Bloomington, 362 pp.

1007 Lewan, M. D., Maynard, J.B., 1982. Factors controlling enrichment of vanadium and nickel in the
1008 bitumen of organic sedimentary rocks. Geochim. Cosmochim. Acta 46, 2547-2560.
1009
1010 Lipinski, M., Warning, B., Brumsack, H.-J., 2003. Trace metal signatures of Jurassic / Cretaceous
1011 black shales from the Norwegian Shelf and the Barents Sea: Palaeogeog. Palaeoclimatol.
1012 Palaeoecol. 190, 459-475.
1013
1014 Ludwig, K.R., 1980. Calculation of uncertainties of U-Pb isotope data. Earth Planet. Sci. Lett. 46,
1015 212-220.
1016
1017 Ludwig, K., 2003, Isoplot/Ex, version 3: a geochronological toolkit for microsoft Excel.:
1018 Geochronology Center Berkeley.
1019
1020 Lüning, S., Adamson, K., Craig, J., 2003. Frasnian organic-rich shales in North Africa: Regional
1021 distribution and depositional model. Spec. Publ.- Geol. Soc. Lond., vol. 207, pp. 165-184.
1022
1023 Lyons, T.W., Berner, R.A., 1992. Carbon-iron-sulfur systematic in the uppermost deep-water
1024 sediments of the Black Sea. Chem. Geol. 99, 1-27.
1025
1026 Martin, C.E., Peucker-Ehrenbrink, B., Brunskill, G., Szymczak, R., 2001. Osmium isotope
1027 geochemistry of a tropical estuary. Geochim. Cosmochim. Acta 65, 3193-3200.
1028

Maynard, J.B., 1980. Sulfur isotopes of iron sulfides in Devonian-Mississippian shales of the Appalachian Basin: control by rate of sedimentation: Am. J. Sci. 280, 772-786.

McLean, R.A., Klapper, G., 1998. Biostratigraphy of Frasnian (Upper Devonian) strata in western Canada, based on conodonts and rugose corals. Bull. Can. Petrol. Geol., 48, 515-563.

Meyer, B.D., Barrick, J.E., 2000. Conodonts from the Woodford Formation (Late Devonian) and adjacent units, subsurface west Texas and eastern New Mexico, in DeMis, W. D., Nelis, M. K., and Trentham, R. C. (Eds.), The Permian Basin: Proving ground for tomorrow's technologies: West Texas Geol. Soc. Pub. 00-109, 229-237.

Mills, R.A., Planquette, H., Pancost, R.D., Hepburn, L., Salter, I., FitzGeorge-Balfour, T., 2011. Quantifying export production in the Southern Ocean: Implications for the Ba_{xs} proxy. Paleoceanography, 26, PA4222, doi: 10.1029/2010PA002111.

Mnich, C.A., 2009. Geochemical signatures of stratigraphic sequences and sea-level change in the Woodford Shale, Permian Basin [M.Sc. thesis]. Golden, Colorado School of Mines, 89 p.

Morford, J.L., Emerson, S., 1999. The geochemistry of redox sensitive trace metals in sediments. Geochim. Cosmochim. Acta 63, 1735-1750.

Mukhopadhyay, B., D. G. Brookins, and S.L. Bolivar, 1975, Rb-Sr whole-rock study of the Precambrian rocks of the Pedernal Hills, New Mexico: Earth and Planetary Science Letters, v. 27, p. 283-286.

Ogg, J. G., G. Ogg, et al. (2008). The concise Geologic Time Scale, Cambridge University Press, 177p.

Peucker-Ehrenbrink, B., Ravizza, G., 2000. The marine osmium isotope record. Terr. Nova 12, 205-219.

Poole, S., Mnich, C.A., Harris, N., Hemmesch, N.T., 2010, Significance of pyrite morphology to the geochemistry and sequence stratigraphy of the Woodford Shale, Permian Basin, west Texas: AAPG Search and Discovery Article #90104.

Rooney, A.D., Chew, D., Selby., D., 2011. Re-Os geochronology of the Neoproterozoic - Cambrian Dalradian Supergroup of Scotland and Ireland: Implications for Neoproterozoic stratigraphy, glaciations and Re-Os systematics. PreCambrian Res. 185, 202-214.

Rooney, A.D., Selby, D., Lewan, M., Lillis, P., Houzay, J.P., 2012. Evaluating Re-Os systematics in organic-rich sedimentary rocks in response to petroleum generation using hydrous pyrolysis experiments. Geochim. Cosmochim. Acta 77, 275-291

1072 Saltzman, M.R., 2005. Phosphorus, nitrogen, and the redox evolution of the Paleozoic oceans:
1073 Geology, v. 33, p. 573-576.
1074
1075 Savoy, L.E., Mountjoy, E.W., 1995. Cratonic-margin and Antler-age foreland basin strata
1076 (Middle Devonian to Lower Carboniferous) of the southern Canadian Rocky Mountains and
1077 adjacent plains. In: Dorobek, S.L., Ross, G.M. (Eds.), Stratigraphic Evolution of Foreland Basins.
1078 Soc. Sediment. Geol. Spec. Publ., v. 52, pp. 213-231.
1079
1080 Schindler, E., 1993. Event-stratigraphic markers within the Kellwasser Crisis near the
1081 Frasnian/Famennian boundary (Upper Devonian) in Germany. Palaeogeog. Palaeoclimatol.
1082 Palaeoecol. 104, 115-125.
1083
1084 Selby, D. 2007. Direct rhenium-osmium age of the Oxfordian-Kimmeridgian boundary, Staffin
1085 Bay, Isle of Skye, UK and the Late Jurassic geologic timescale. Nor. J. Geol., 87, 291-299
1086
1087 Selby, D., Creaser, R.A., 2003. Re-Os geochronology of organic rich sediments: An evaluation of
1088 organic matter analysis methods. Chem. Geol. 200, 225-240.
1089
1090 Selby, D., Creaser, R.A., 2005. Direct radiometric dating of the Devonian-Mississippian time-
1091 scale boundary using the Re-Os black shale geochronometer. Geology, 33, 545-548.
1092

1093 Selby, D., Mutterlose, J., and Condon, D.J. 2009. U-Pb and Re-Os Geochronology of the
1094 Aptian/Albian and Cenomanian/Turonian stage boundaries: Implications for timescale
1095 calibration, osmium isotope seawater composition and Re-Os systematics in organic-rich
1096 sediments. Chemical Geology, 265, 394-409.
1097
1098 Smoliar, M.I., Walker, R.J., Morgan, J.W., 1996. Re-Os isotope constraints on the age of Group
1099 IIA, IIIA, IVA, and IVB iron meteorites. Science 271, 1099-1102.
1100
1101 Swan, A.R.H., Sandilands, M., 1995. Introduction to geological data analysis: Blackwell-Science,
1102 Oxford, 446 pp.
1103
1104 Tissot, B. P. and D. H. Welte. 1984. Petroleum Formation and Occurrence, Second Revised and
1105 Enlarged Edition. Springer-Verlag, Berlin, pp. 699.
1106
1107 Tribovillard, N., Algeo, T.J., Lyons, T., Riboulleau, A., 2006. Trace metals as paleoredox and
1108 paleoproductivity proxies: An update. Chem. Geol. 232, 12-32.
1109
1110 Tribovillard, N., Bout-Roumazeilles, B., Algeo, T.J., Lyons, T., Sionneau, T., Montero-Serrano,
1111 J.C., Riboulleau, A., Baudin, F., 2008. Paleodepositional conditions in the Orca Basin as inferred
1112 from organic matter and trace metal contents. Mar. Geol. 254, 62-72.
1113

1114 Turgeon, S.C., Creaser, R.A., Algeo, T.J., 2007. Re-Os depositional dates and seawater Os for the
1115 Frasnian–Famennian boundary: Implications for weathering rates, land plant evolution, and
1116 extinction mechanisms. Earth Planet. Sci. Lett. 261, 649-661.
1117
1118 Warning, B., Brumsack, H.-J., 2000. Trace metal signatures of Mediterranean sapropels:
1119 Palaeogeog. Palaeoclimatol. Palaeoecol. 158, 293-309.
1120
1121 Wedepohl, K.H., 1991, The composition of the upper Earth's crust and the natural cycles of
1122 selected metals, in Merian, E. (Ed.), Metals and their Compounds in the Environment: BCH-
1123 Verlagsgesellschaft, Weinheim, pp. 3-17.
1124
1125 Yamashita, Y., Takahashi, Y., Haba, H., Enomoto, S., Shimizu, H., 2007. Comparison of reductive
1126 accumulation of Re and Os in seawater-sediment systems. Geochim. Cosmochim. Acta 71,
1127 3458-3475.

FIGURE CAPTIONS

Figure 1. A. Map of configuration of the continents at 370 Ma, modified after Blakey (2012), showing locations of Middle and Upper Devonian organic-rich shale formations. Location of North African shale formations from Luning et al (2003) and Australian and eastern European occurrences after Klemme and Ulmishek (1991). B. North American continent at 365 Ma, modified after Blakey (2012). Sedimentary basins with Middle or Upper Devonian organic-rich shale formations are highlighted. C. Map of the Permian Basin, showing the locations of the two cores described here. Modified after Comer (1991).

Figure 2. Gamma ray logs for the (A) Pecos County and (B) Winkler County wells, showing stratigraphic subdivisions of the Woodford. Solid bars indicate cored and sampled intervals.

Figure 3. Description of the Woodford Shale core from the Pecos County well, showing lithologies, gamma logs TOC data and organic matter type. Modified after Hemmesch et al. (in press).

Figure 4. Description of the Woodford Shale core from the Winkler County well, showing lithologies, gamma logs, and TOC data. Modified after Hemmesch et al. (in press).

Figure 5. A. Hydrogen and oxygen index data for samples from the Winkler and Pecos County wells. B. Thermal maturity data (Tmax from Rockeval analysis) from the Winkler and Pecos County wells.

Figure 6. Enrichment factors for minor and trace elements. Sections of each bar represent quartiles of the sample population.

Figure 7. Geochemical profiles for the Pecos and Winkler County wells. Note that the cored interval in the Winkler County well only includes the Middle Woodford and the lowermost part of the Upper Woodford sections. Points of stratigraphic correlation between the two wells

based on the gamma logs and the V/Al_2O_3 and Mo/Al_2O_3 curves are identified by letters along the right side of the plots.

Figure 8. Re and ^{192}Os abundance and Os_i values for the four sample sets from the Pecos County well.

Figure 9. Re-Os isotope data for all four analysed sections from the Pecos County well illustrating the variation in the $^{187}Re/^{188}Os$ and $^{187}Os/^{188}Os$ values between each interval

Figure 10. $^{187}Re/^{188}Os$ vs $^{187}Os/^{188}Os$ isochron plots for the four selected horizons. See text for discussion.

Figure 11. Cross-plots of geochemical data. (A) and (B) U, Mo, and V content versus TOC for the Pecos County and Winkler County wells. Data from the two wells are separated because of differences in TOC content, resulting from hydrocarbon generation and expulsion. Uranium and Mo exhibit strong correlations with TOC, whereas V does not. (C) Mo/Al_2O_3 versus TOC/P_{tot} for the Pecos County and Winkler County wells. Some Upper Woodford samples have low TOC/P_{tot},indicating more oxidizing water column conditions. (D) Cu versus Ni values for the Woodford samples. Formation is generally depleted in Cu relative to other black shale formations.

TABLE CAPTIONS

Table 1. Multipliers relating raw enrichment factors to Al-normalized enrichment factors.

Table 2. Factor analysis results for major, minor and trace elements in the Pecos and Winkler County wells.

Table 3. Table 2: Re-Os data for four sections of the Pecos County core

Figure 1

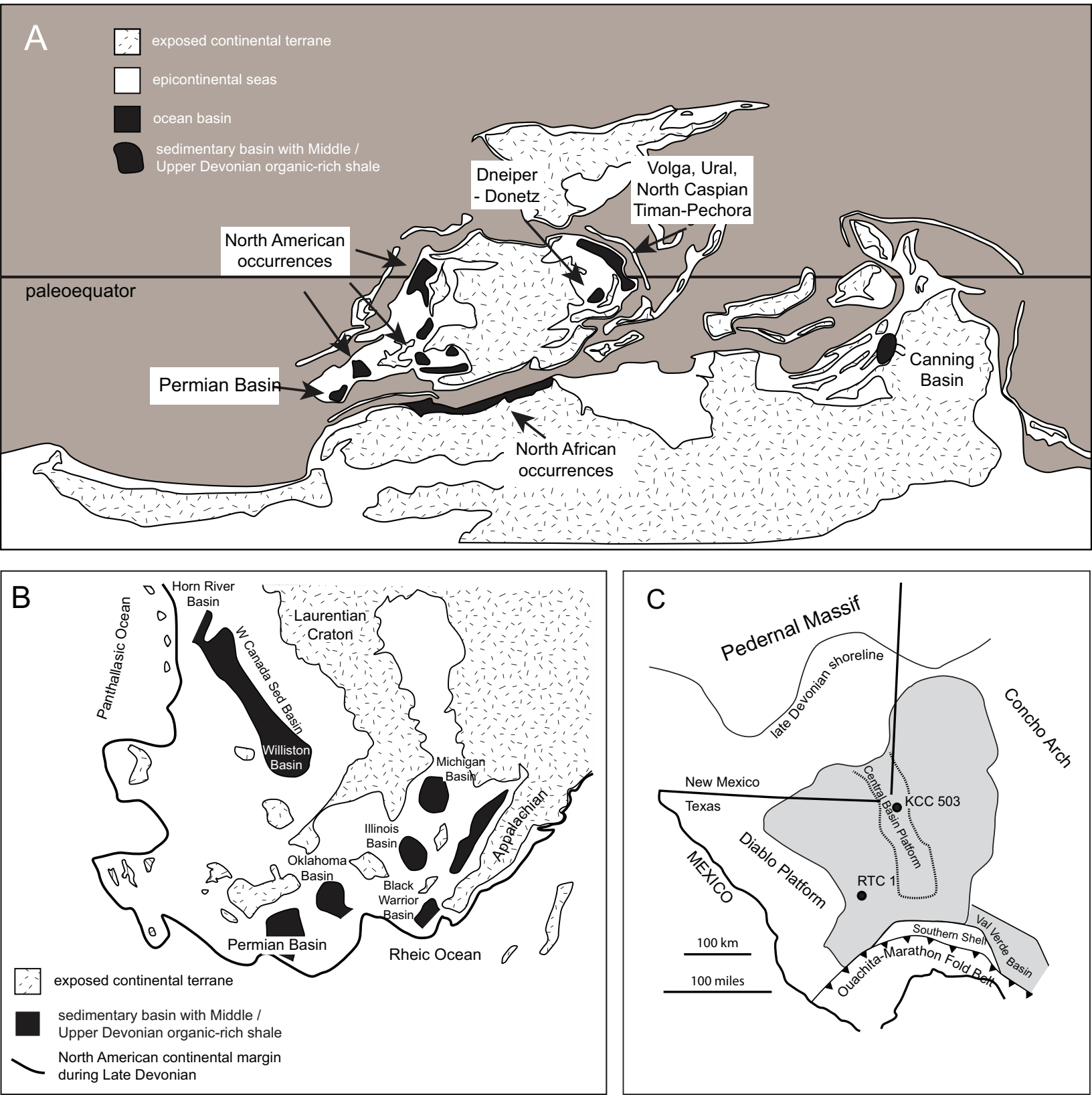
A
exposed continental terrane
epicontinental seas
ocean basin
sedimentary basin with Middle / Upper Devonian organic-rich shale
Dneiper - Donetz
Volga, Ural, North Caspian Timan-Pechora
North American occurrences
paleoequator
Permian Basin
Canning Basin
North African occurrences
B
Horn River Basin
Panthallasic Ocean
W Canada Sed Basin
Laurentian Craton
Williston Basin
Michigan Basin
Illinois Basin
Appalachian
Oklahoma Basin
Black Warrior Basin
Permian Basin
Rheic Ocean
exposed continental terrane
sedimentary basin with Middle / Upper Devonian organic-rich shale
North American continental margin during Late Devonian
C
Pedernal Massif
late Devonian shoreline
Concho Arch
New Mexico
Texas
Central Basin Platform
KCC 503
Diablo Platform
MEXICO
RTC 1
Val Verde Basin
Southern Shelf
Ouachita-Marathon Fold Belt
100 km
100 miles

Figure 2

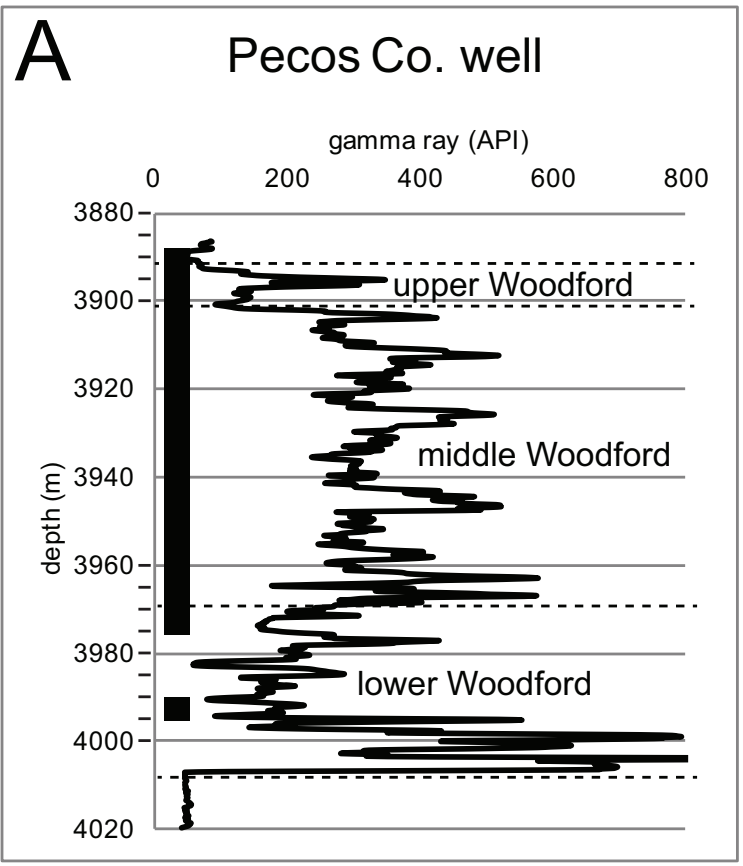
A
Pecos Co. well
gamma ray (API)
0
200
400
600
800
depth (m)
3880
3900
3920
3940
3960
3980
4000
4020
upper Woodford
middle Woodford
lower Woodford

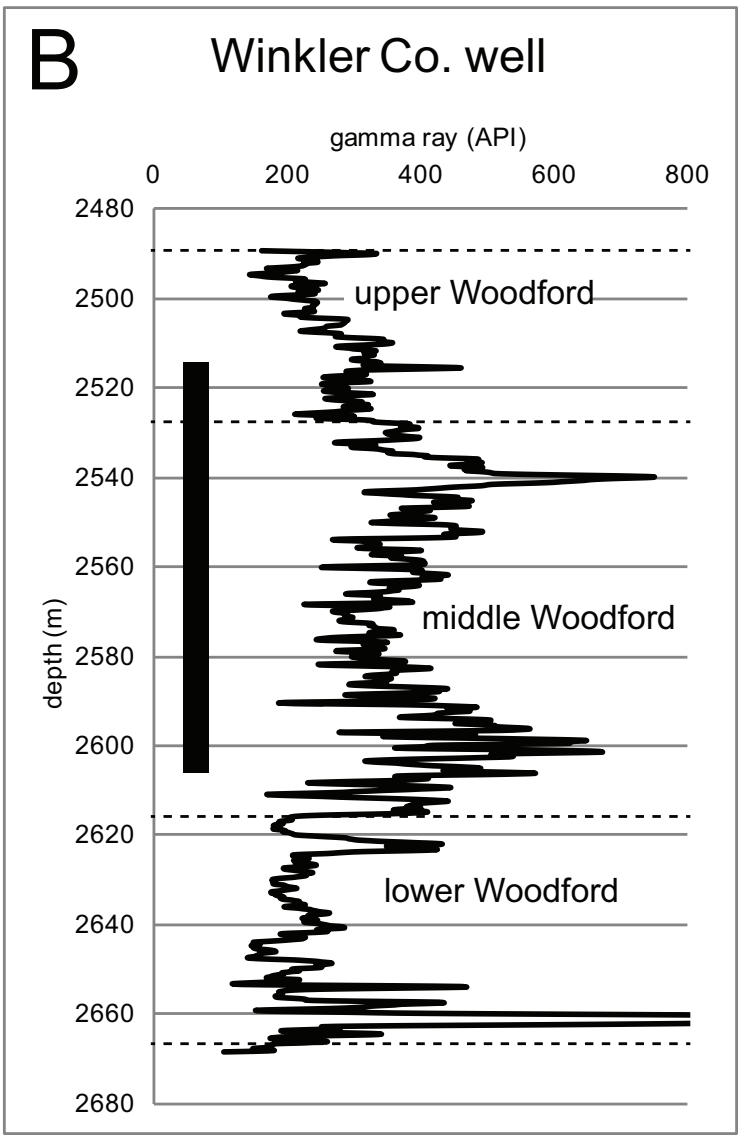
B
Winkler Co. well
gamma ray (API)
0
200
400
600
800
depth (m)
2480
2500
2520
2540
2560
2580
2600
2620
2640
2660
2680
upper Woodford
middle Woodford
lower Woodford

Figure 3

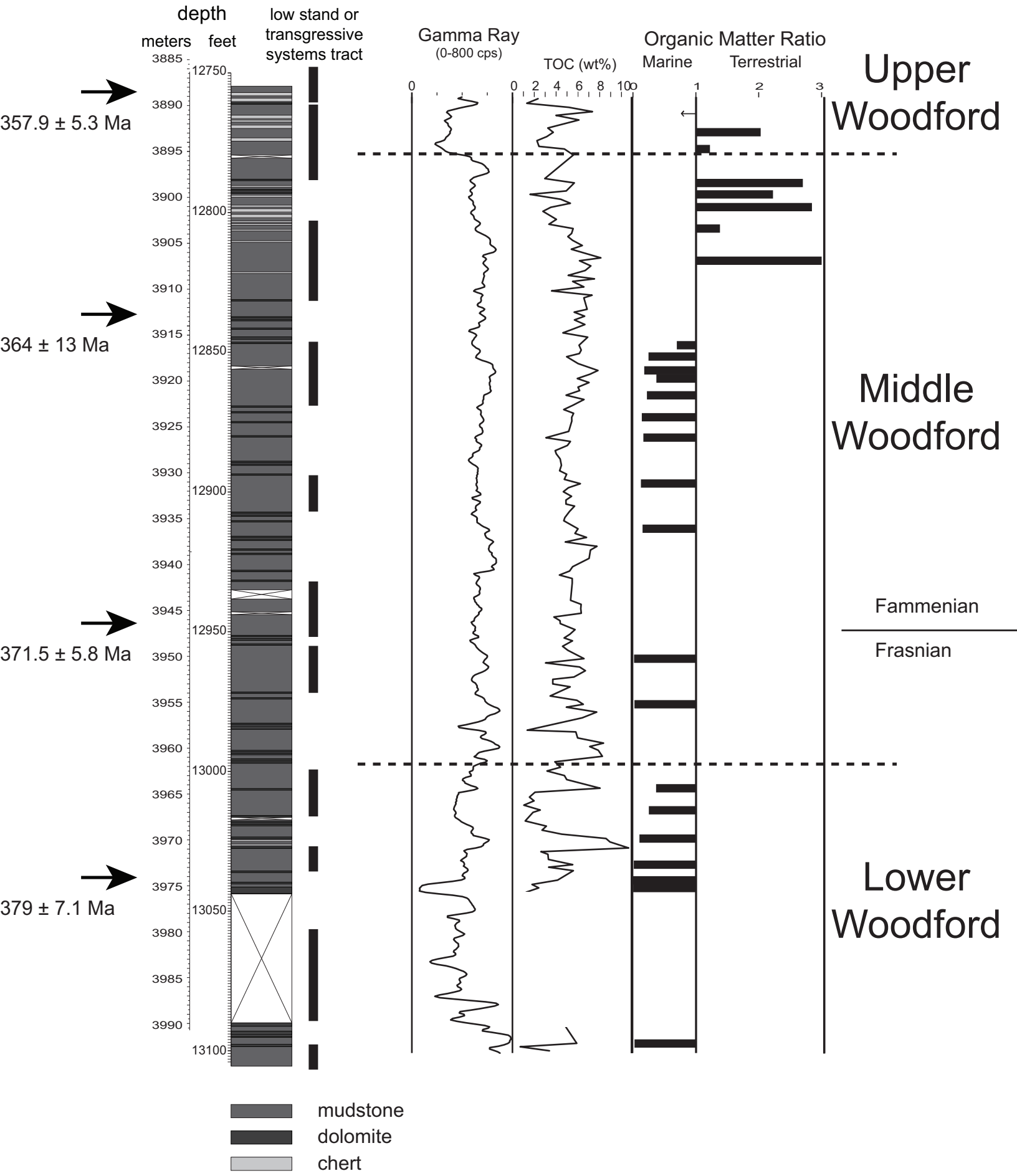
depth
meters
feet
low stand or transgressive systems tract
Gamma Ray
(0-800 cps)
TOC (wt%)
Organic Matter Ratio
Marine
Terrestrial
Upper Woodford
Middle Woodford
Lower Woodford
Fammenian
Frasnian
357.9 ± 5.3 Ma
364 ± 13 Ma
371.5 ± 5.8 Ma
379 ± 7.1 Ma
mudstone
dolomite
chert

Figure 4

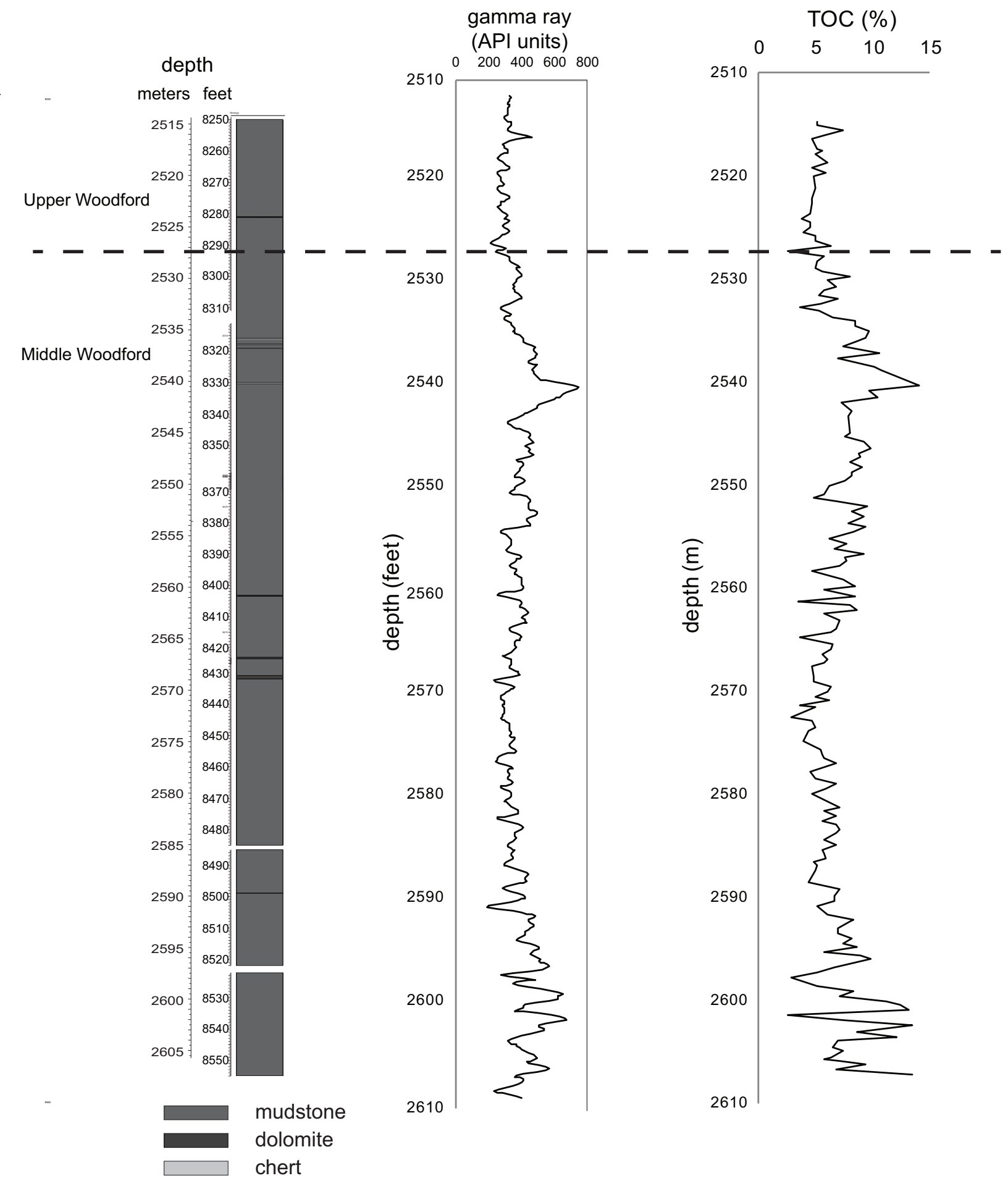
depth
meters
feet
Upper Woodford
Middle Woodford
gamma ray
(API units)
0 200 400 600 800
depth (feet)
TOC (%)
0 5 10 15
depth (m)
mudstone
dolomite
chert

Figure 5

A

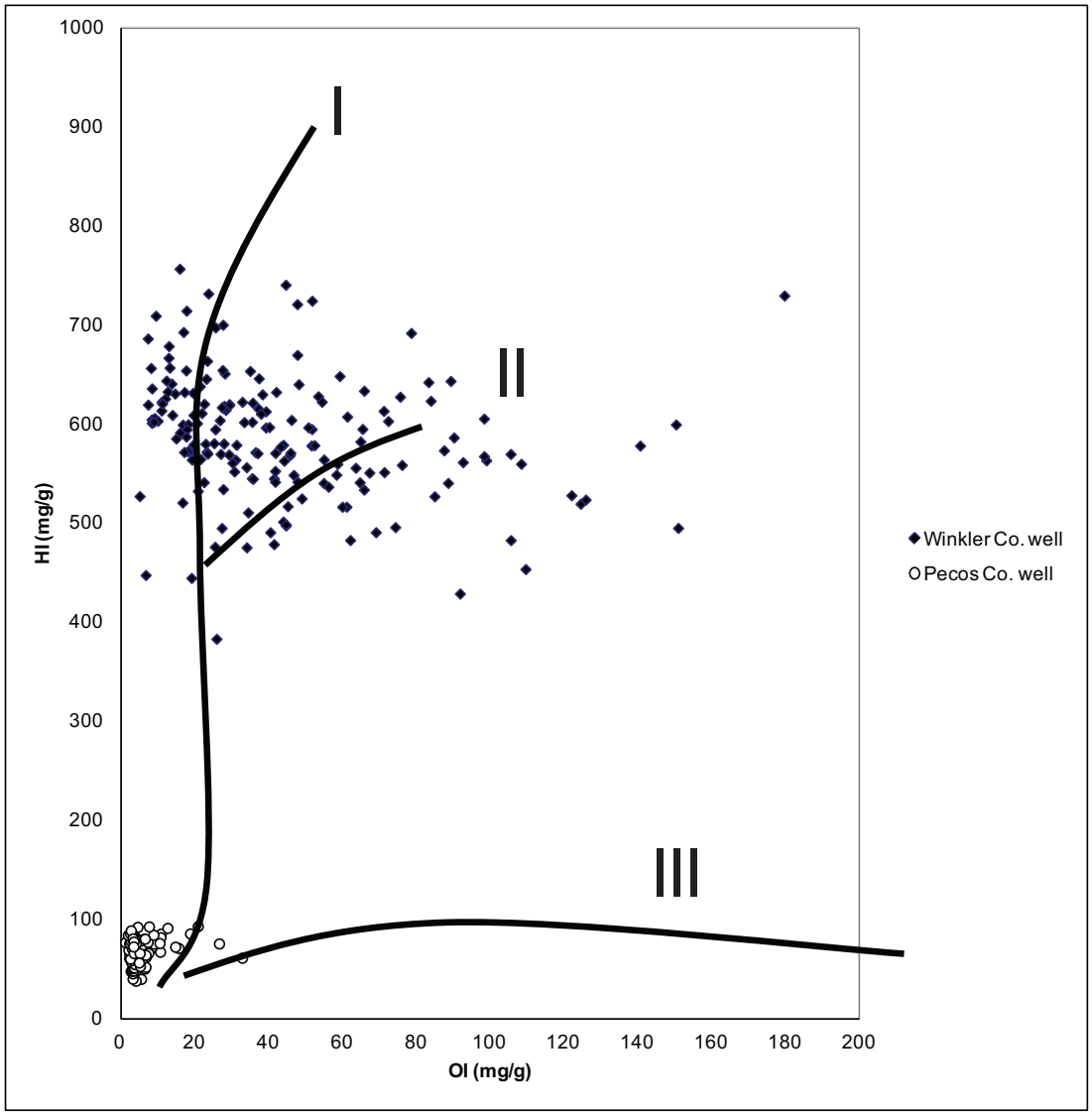
1000
900
800
700
600
500
400
300
200
100
0
HI (mg/g)
0
20
40
60
80
100
120
140
160
180
200
OI (mg/g)
I
II
III
Winkler Co. well
Pecos Co. well

B

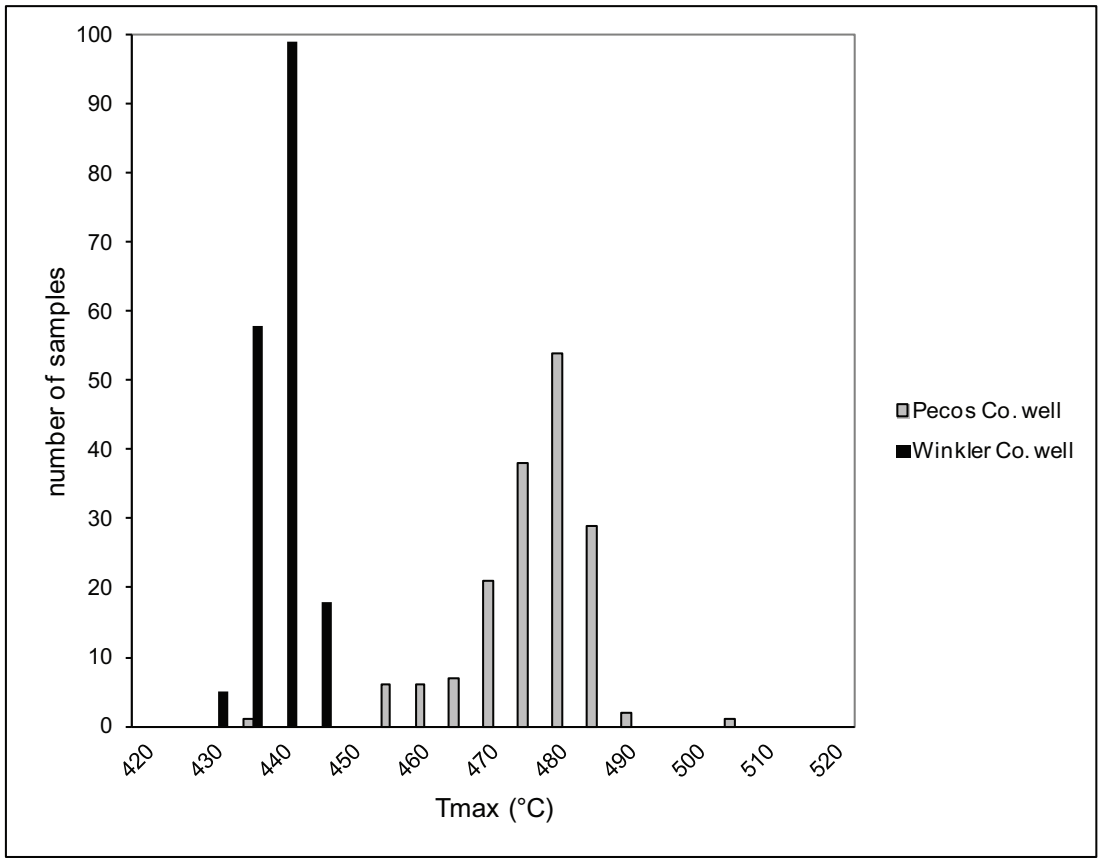
100
90
80
70
60
50
40
30
20
10
0
number of samples
420
430
440
450
460
470
480
490
500
510
520
Tmax (°C)
Pecos Co. well
Winkler Co. well

Figure 6

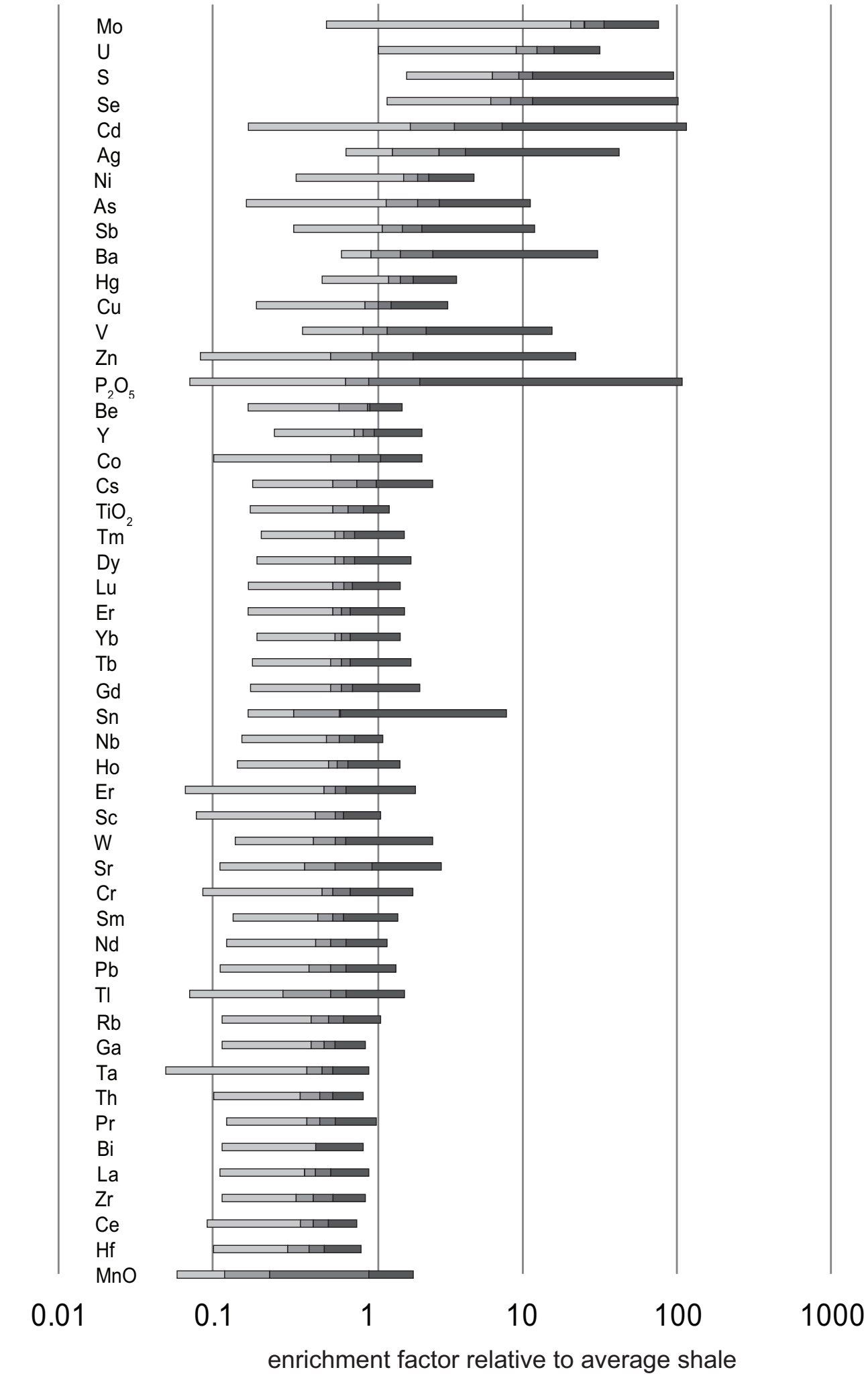
Mo
U
S
Se
Cd
Ag
Ni
As
Sb
Ba
Hg
Cu
V
Zn
P_2O_5
Be
Y
Co
Cs
TiO_2
Tm
Dy
Lu
Er
Yb
Tb
Gd
Sn
Nb
Ho
Er
Sc
W
Sr
Cr
Sm
Nd
Pb
Tl
Rb
Ga
Ta
Th
Pr
Bi
La
Zr
Ce
Hf
MnO
0.01
0.1
1
10
100
1000
enrichment factor relative to average shale

Figure 7

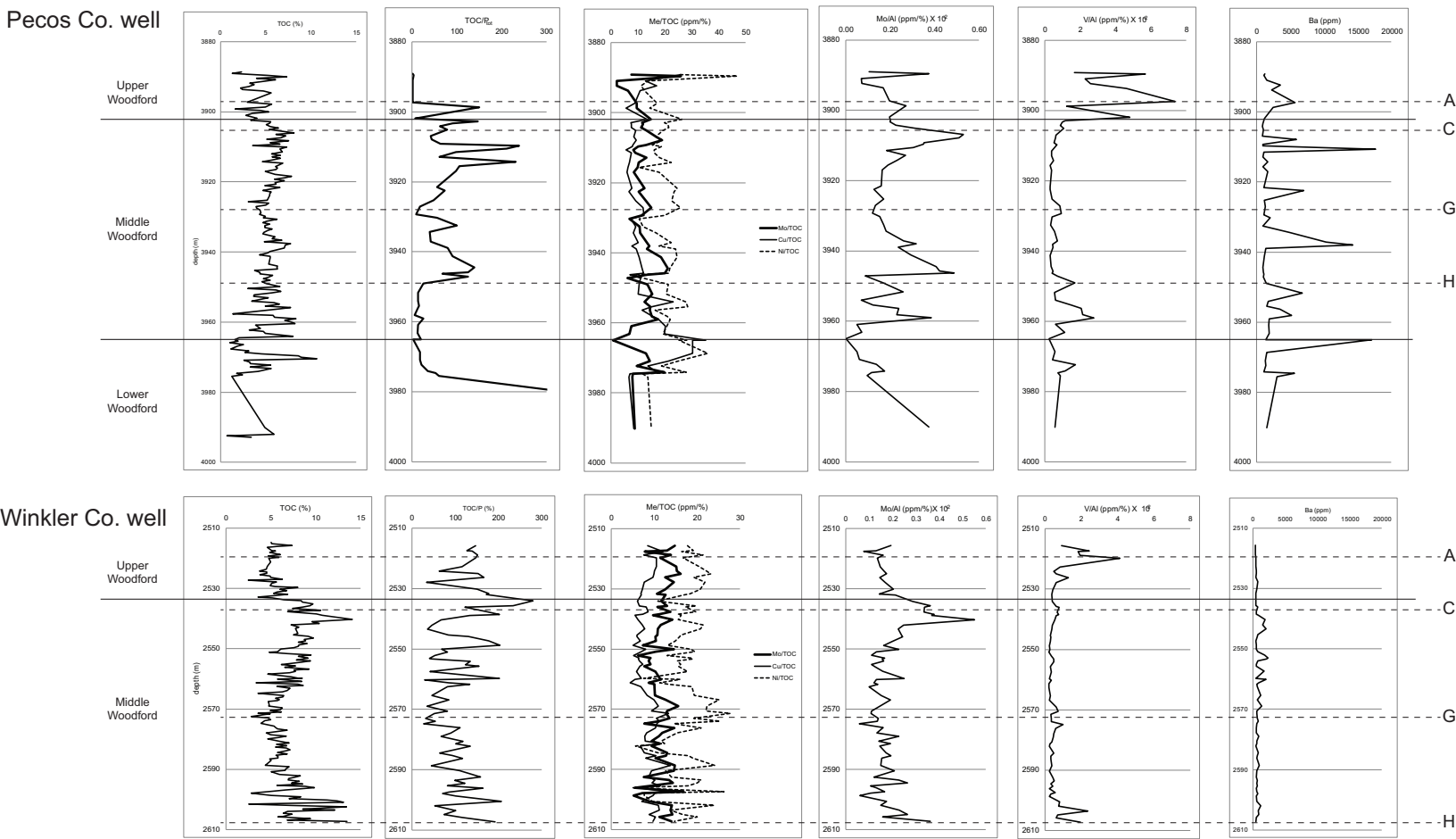
Pecos Co. well
Upper Woodford
Middle Woodford
Lower Woodford
depth (m)
TOC (%)
TOC/P (%)
Me/TOC (ppm/%)
Mo/Al (ppm/%) X 10²
V/Al (ppm/%) X 10²
Ba (ppm)
Mo/TOC
Cu/TOC
Ni/TOC
A
C
G
H
Winkler Co. well
Upper Woodford
Middle Woodford
depth (m)
TOC (%)
TOC/P (%)
Me/TOC (ppm/%)
Mo/Al (ppm/%)X 10²
V/Al (ppm/%) X 10²
Ba (ppm)
Mo/TOC
Cu/TOC
Ni/TOC
A
C
G
H

Figure 8

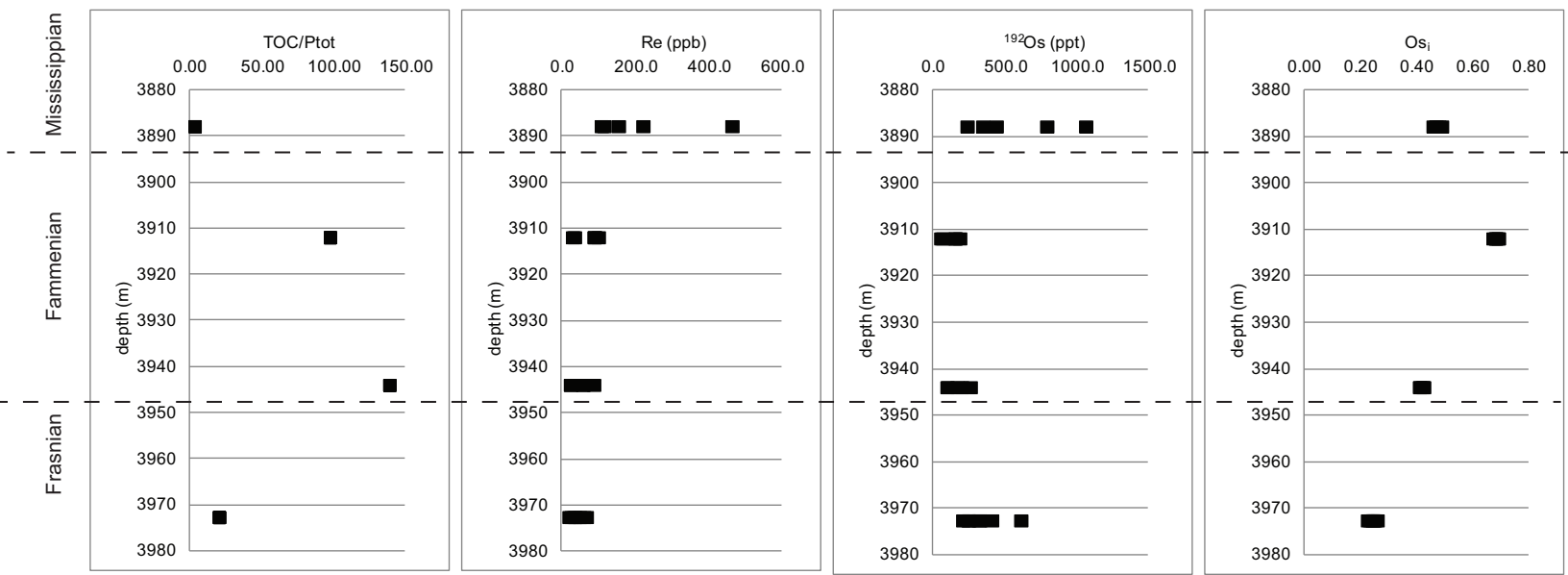
Mississippian
Fammenian
Frasnian
TOC/Ptot
0.00
50.00
100.00
150.00
Re (ppb)
0.0
200.0
400.0
600.0
192Os (ppt)
0.0
500.0
1000.0
1500.0
Osi
0.00
0.20
0.40
0.60
0.80
depth (m)
3880
3890
3900
3910
3920
3930
3940
3950
3960
3970
3980

Figure 9

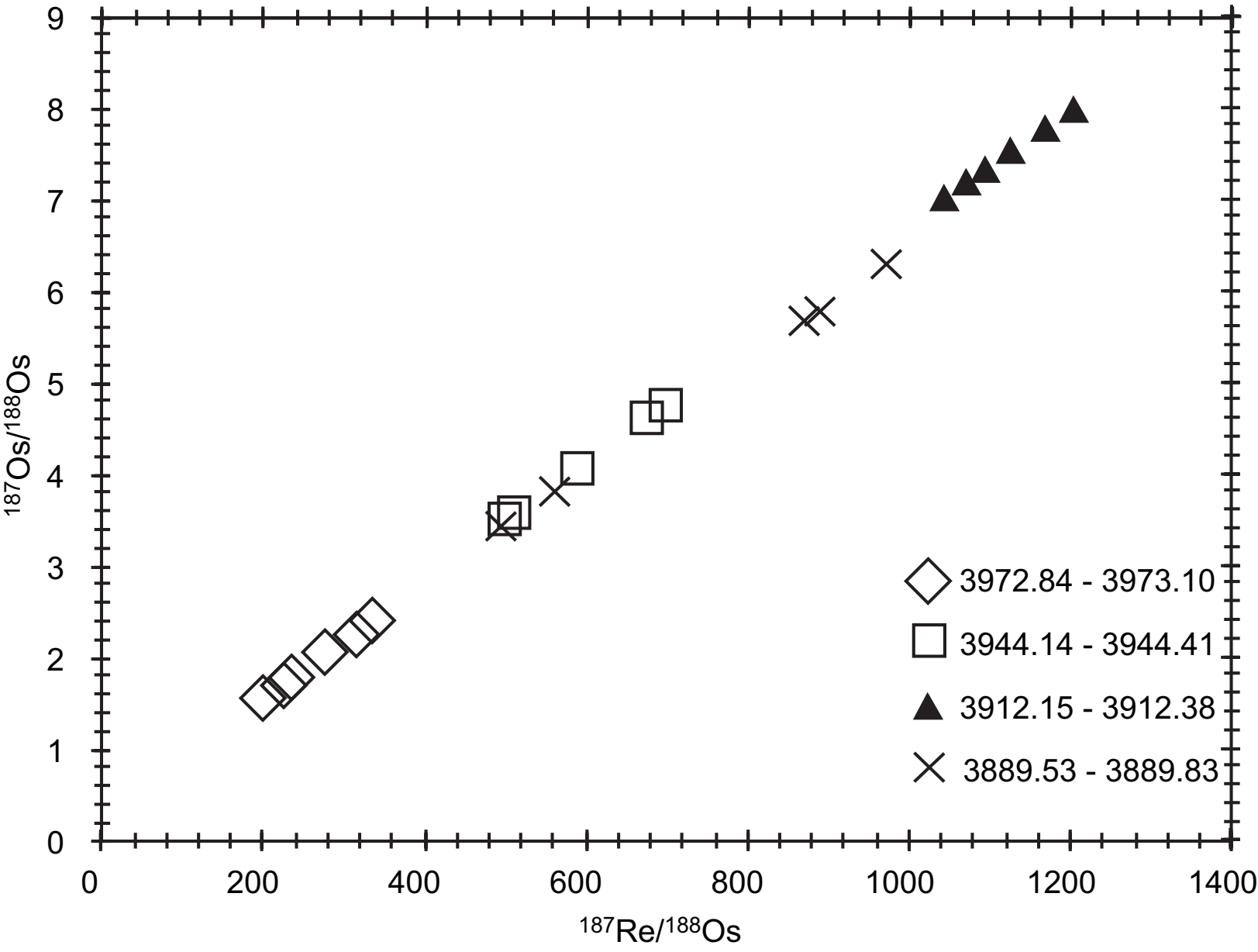
9
8
7
6
5
4
3
2
1
0
0
200
400
600
800
1000
1200
1400
$^{187}Os/^{188}Os$
$^{187}Re/^{188}Os$
3972.84 - 3973.10
3944.14 - 3944.41
3912.15 - 3912.38
3889.53 - 3889.83

Figure 10

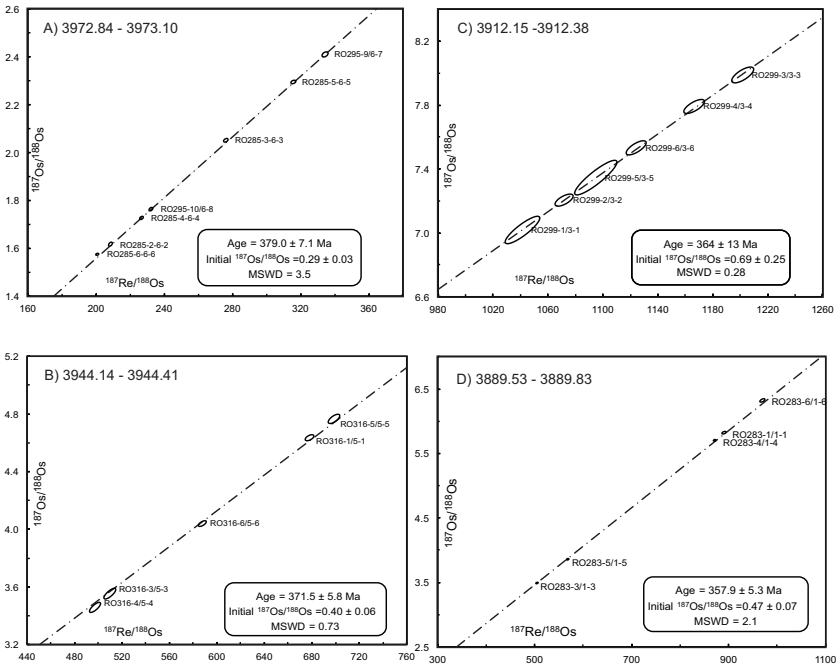
A) 3972.84 - 3973.10
RO295-9/6-7
RO285-5-6-5
RO285-3-6-3
RO295-10/6-8
RO285-4-6-4
RO285-2-6-2
RO285-6-6-6
Age = 379.0 ± 7.1 Ma
Initial 187Os/188Os =0.29 ± 0.03
MSWD = 3.5
187Os/188Os
187Re/188Os
C) 3912.15 -3912.38
RO299-3/3-3
RO299-4/3-4
RO299-6/3-6
RO299-5/3-5
RO299-2/3-2
RO299-1/3-1
Age = 364 ± 13 Ma
Initial 187Os/188Os =0.69 ± 0.25
MSWD = 0.28
B) 3944.14 - 3944.41
RO316-5/5-5
RO316-1/5-1
RO316-6/5-6
RO316-3/5-3
RO316-4/5-4
Age = 371.5 ± 5.8 Ma
Initial 187Os/188Os =0.40 ± 0.06
MSWD = 0.73
D) 3889.53 - 3889.83
RO283-6/1-6
RO283-1/1-1
RO283-4/1-4
RO283-5/1-5
RO283-3/1-3
Age = 357.9 ± 5.3 Ma
Initial 187Os/188Os =0.47 ± 0.07
MSWD = 2.1

Figure 11

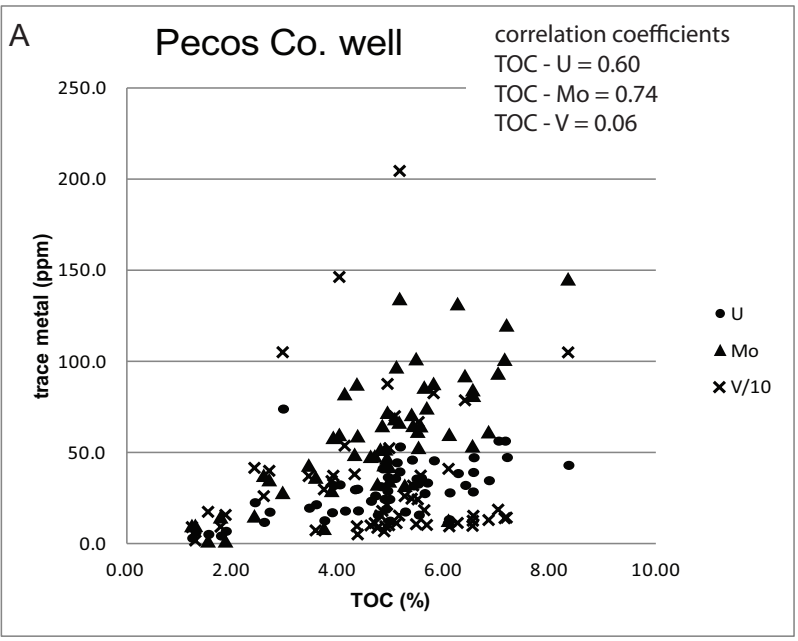
A
Pecos Co. well
correlation coefficients
TOC - U = 0.60
TOC - Mo = 0.74
TOC - V = 0.06
trace metal (ppm)
250.0
200.0
150.0
100.0
50.0
0.0
0.00
2.00
4.00
6.00
8.00
10.00
TOC (%)
U
Mo
V/10

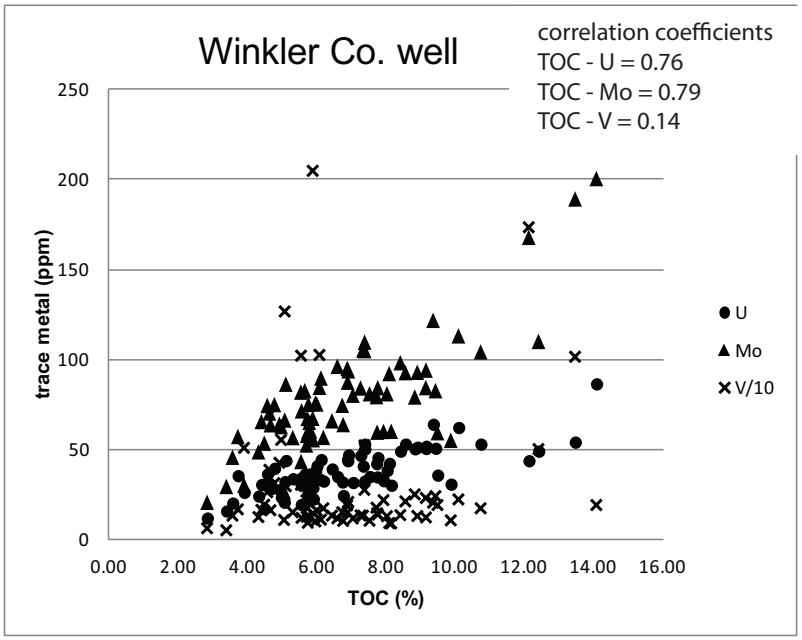
Winkler Co. well
correlation coefficients
TOC - U = 0.76
TOC - Mo = 0.79
TOC - V = 0.14
trace metal (ppm)
250
200
150
100
50
0
0.00
2.00
4.00
6.00
8.00
10.00
12.00
14.00
16.00
TOC (%)
U
Mo
V/10

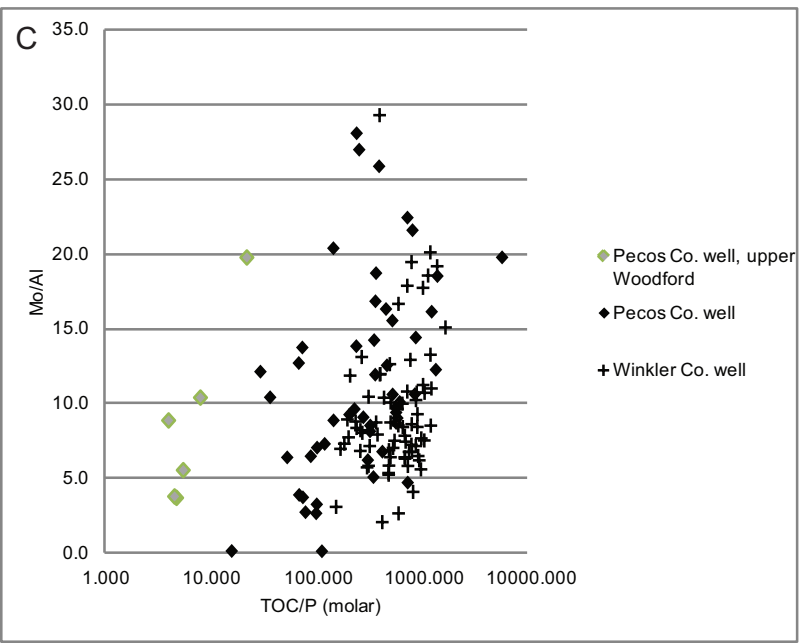
C
Mo/Al
35.0
30.0
25.0
20.0
15.0
10.0
5.0
0.0
1.000
10.000
100.000
1000.000
10000.000
TOC/P (molar)
Pecos Co. well, upper Woodford
Pecos Co. well
Winkler Co. well

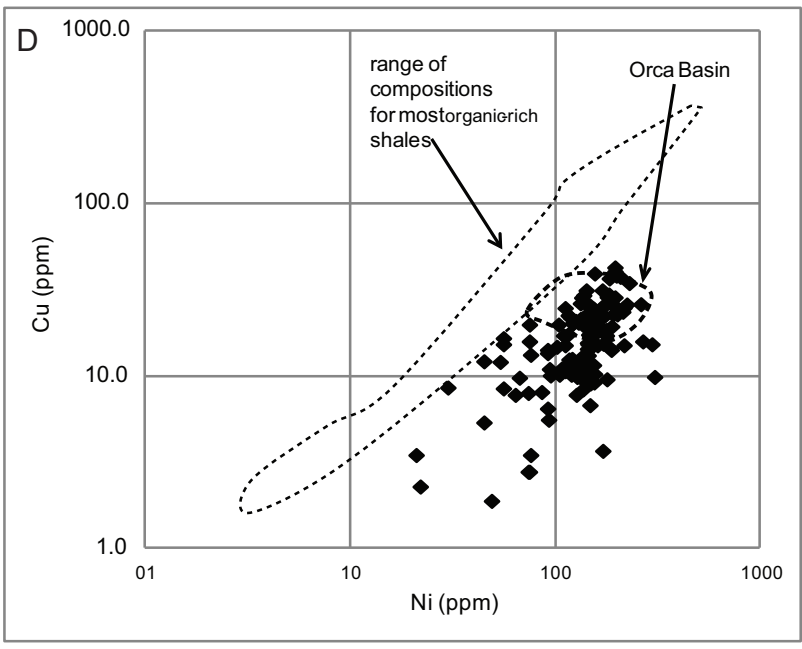
D
Cu (ppm)
1000.0
100.0
10.0
1.0
01
10
100
1000
Ni (ppm)
range of compositions for most organic-rich shales
Orca Basin

Table 1

Click here to download Table: Harris et al revised Table 1.docx

	min	25%ile	50%ile	75%ile	max	mean
MnO	1.072	1.082	0.909	1.275	2.400	1.599
Hf	2.654	1.508	1.175	1.027	0.934	1.201
Ce	3.260	1.313	1.231	1.146	1.296	1.246
Zr	2.442	1.449	1.205	1.007	0.934	1.210
La	2.775	1.309	1.270	1.242	1.425	1.273
Bi	1.496	1.706	1.916	2.197	1.496	1.943
Pr	2.561	1.332	1.249	1.174	1.235	1.266
Th	2.764	1.474	1.184	1.013	0.934	1.196
Ta	4.582	1.293	1.141	1.072	1.068	1.211
Ga	2.068	1.384	1.181	1.066	0.888	1.220
Rb	2.325	1.470	1.187	0.985	0.866	1.187
Tl	0.646	1.147	1.140	1.367	2.002	1.359
Pb	2.303	1.361	1.202	1.206	0.927	1.241
Nd	2.780	1.378	1.201	1.167	1.269	1.269
Sm	2.350	1.339	1.223	1.231	1.231	1.291
Cr2O3	2.670	1.289	1.249	1.199	2.599	1.309
Sr	2.040	1.274	1.128	1.196	4.582	1.621
W	1.072	1.259	1.270	1.224	1.450	1.301
Sc	3.791	1.425	1.155	1.108	2.479	1.249
Eu	4.238	1.264	1.230	1.265	1.273	1.305
Ho	2.797	1.133	1.192	1.330	2.130	1.351
Nb	2.342	1.441	1.209	1.025	0.893	1.211
Sn	0.948	1.359	0.863	1.021	1.450	1.252
Gd	1.947	1.238	1.249	1.326	1.663	1.334
Tb	2.082	1.209	1.216	1.339	2.237	1.347
Yb	2.542	1.156	1.198	1.293	2.233	1.332
Er	2.880	1.160	1.179	1.341	2.061	1.345
Lu	2.913	1.203	1.195	1.290	2.272	1.335
Dy	2.277	1.174	1.213	1.303	2.227	1.347
Tm	2.266	1.160	1.163	1.325	2.176	1.348
TiO2	2.132	1.428	1.214	0.990	0.934	1.203
Cs	2.001	1.478	1.197	1.075	0.669	1.168
Co	3.351	1.300	1.318	1.190	1.061	1.240
Y	2.414	1.141	1.209	1.371	2.719	1.380
Be	2.211	1.178	0.951	1.278	1.602	1.271
P2O5	4.059	1.131	1.327	1.211	2.617	2.564
Zn	1.018	1.347	1.247	1.326	1.582	1.410
Cu	3.215	1.197	1.188	1.337	1.764	1.334
V	1.219	1.328	1.332	1.279	1.695	1.313
Hg	4.582	1.080	1.147	1.223	3.882	1.327
Ba	0.844	1.136	1.315	1.296	2.670	1.734
Sb	0.749	1.156	1.209	1.538	2.803	1.531
As	1.177	1.236	1.260	1.287	2.011	1.375
Ni	1.207	1.139	1.214	1.366	1.307	1.323
Ag	1.937	1.441	1.427	1.276	1.307	1.399
Ni	1.354	1.225	1.193	1.364	1.453	1.328
Cd	1.937	1.441	1.427	1.276	1.307	1.399
Se	2.132	1.141	1.144	1.287	2.559	1.647
S	0.970	0.754	0.689	0.742	2.218	0.843

U	1.070	1.240	1.229	1.232	2.831	1.378
Mo	0.646	1.185	1.206	1.297	1.300	1.327

Table 2

Click here to download Table: Harris et al revised Table 2.docx

	Factor												
	1		2		3		4		5		6		7
%age of total variance	39.00%		13.00%		11.00%		7.90%		6.30%		3.60%		3.60%
Al2O3	.945	Y	.935	TOC	.817	SiO2	-.923	V	.813	Fe2O3	.970	P2O5	.838
Na2O	.828	La	.692	Ni	.787	MgO	.934	Cd	.921	TOTAL S	.963	Ag	.643
K2O	.937	Ce	.504	Co	.675	CaO	.883	Sb	.759	As	.563	Se	.553
TiO2	.952	Pr	.720	U	.860	MnO	.853	Ag	.683	Hg	.575		
Cr2O3	.547	Nd	.733	Mo	.830	LOI	.898	Se	.701				
Cs	.805	Sm	.834	Ni	.827	Sr	.583						
Ga	.920	Eu	.886	As	.729	inorganic C	.880						
Hf	.921	Gd	.941	Hg	.615								
Nb	.931	Tb	.944	Tl	.716								
Rb	.918	Dy	.931										
Ta	.900	Ho	.925										
Th	.930	Er	.894										
Zr	.915	Tm	.863										
La	.575	Yb	.817										
Ce	.680	Lu	.798										
Pr	.577												
Nd	.541												
Pb	.628												
Bi	.779												

a. Rotation converged in 11 iterations.

Table 3

Click here to download Table: Harris et al revised Table 3.docx

Batch/Sample	Re (ppb)	±	Os (ppt)	±	^{192}Os (ppt)	±	^{187}Re/^{188}Os	±	^{187}Os/^{188}Os	±	rho[a]		Os_i[b]
Section D: ~358Ma													
12760.95-12761.90 ft													
RO283-1/1-1	156.9	0.5	1476.0	6.8	350.3	0.8	891.3	3.5	5.7972	0.0155	0.463		0.47
RO283-3/1-3	110.5	0.4	1538.8	6.3	443.4	1.0	495.6	1.9	3.4441	0.0096	0.428		0.48
RO283-4/1-4	466.8	1.5	4447.0	17.2	1064.9	1.5	872.0	3.1	5.6777	0.0109	0.278		0.46
RO283-5/1-5	223.8	0.7	2851.0	10.2	794.4	1.2	560.4	2.0	3.8192	0.0077	0.303		0.47
RO283-6/1-6	117.8	0.4	1054.2	5.8	241.0	0.7	972.3	4.3	6.3052	0.0226	0.586		0.49
average	215.2				578.8								
1 SD	147.7				341.9								
Section C: ~364Ma													
12835.15-12835.90 ft													
RO299-1/3-1	37.0	0.1	325.2	3.1	70.7	0.7	1041.8	10.2	7.0181	0.0698	0.869		0.68
RO299-2/3-2	102.1	0.3	882.7	5.5	189.5	0.7	1072.6	5.4	7.2071	0.0320	0.661		0.68
RO299-3/3-3	91.4	0.3	741.6	5.1	151.2	0.7	1202.7	6.6	7.9887	0.0402	0.710		0.67
RO299-4/3-4	92.2	0.3	760.9	5.0	157.1	0.7	1167.4	6.2	7.7937	0.0366	0.713		0.69
RO299-5/3-5	31.9	0.1	272.5	2.9	57.9	0.7	1095.5	12.7	7.3470	0.0877	0.893		0.68
RO299-6/3-6	90.6	0.3	763.3	5.0	160.3	0.7	1125.2	6.1	7.5346	0.0363	0.715		0.69
average	74.2				131.1								
1 SD	31.1				53.5								
Section B: ~370Ma													
12940.10-12941.00 ft													
RO316-1/5-1	89.5	0.3	1009.1	5.2	262.9	0.8	677.2	3.0	4.6110	0.0172	0.559		0.42
RO316-3/5-3	26.1	0.1	357.1	2.6	101.6	0.7	510.9	4.0	3.5850	0.0291	0.774		0.43
RO316-4/5-4	26.7	0.1	372.2	2.7	106.8	0.7	498.4	3.8	3.4934	0.0279	0.767		0.41
RO316-5/5-5	59.8	0.2	661.8	4.0	170.7	0.7	697.5	3.7	4.7334	0.0237	0.675		0.42
RO316-6/5-6	59.9	0.2	741.7	3.7	202.6	0.7	587.7	2.8	4.0464	0.0154	0.646		0.41
average	52.4				168.9								
1 SD	26.6				67.8								
Section A: ~380 Ma													
13034.25-13035.10 ft													
RO285-2/6-2	22.2	0.1	609.4	2.3	210.7	0.6	209.4	0.9	1.6172	0.0062	0.470		0.25
RO285-3/6-3	35.2	0.1	765.3	2.8	252.5	0.6	276.9	1.1	2.0524	0.0064	0.425		0.25
RO285-4/6-4	28.3	0.1	724.0	2.5	247.3	0.6	227.7	0.9	1.7279	0.0052	0.419		0.24
RO285-5/6-5	50.7	0.2	990.1	3.4	318.6	0.6	316.4	1.2	2.2974	0.0059	0.364		0.24
RO285-6/6-6	62.3	0.2	1768.5	5.2	614.1	1.0	201.8	0.7	1.5760	0.0039	0.311		0.26
RO295-9/6-7	69.3	0.2	1292.7	5.3	411.2	1.0	335.2	1.3	2.4115	0.0082	0.419		0.23
RO295-10/6-8	38.6	0.1	966.3	3.3	328.7	0.7	233.4	0.9	1.7647	0.0053	0.424		0.24
average	43.8				340.4								
1 SD	17.6				137.7								
Duvernay Formation, Canada, Frasian ~378 Ma[c]													
DS45-03-1-7	7.9	0.0	217.4	0.9	74.5	0.2	212.1	1.0	1.6955	0.0070	0.483		0.36
DS45-03-3-1	7.7	0.0	206.4	1.0	70.5	0.3	218.1	1.1	1.7270	0.0101	0.504		0.35
DS45-03-6-1	8.8	0.0	219.6	1.0	74.0	0.2	237.5	1.1	1.8553	0.0084	0.482		0.35
Hangenberg Black Shale, Germany: Upper Famennian[d]													
19-1	33.4	0.1	262.1	2.3	53.1	0.3	1248.7	7.5	8.0670	0.0594	0.577		0.42
19-14	39.0	0.1	397.2	2.3	98.2	0.3	790.4	3.4	5.2611	0.0230	0.427		0.42
19-16	45.4	0.1	487.6	3.5	124.5	0.5	725.2	3.9	4.8581	0.0320	0.511		0.41

All uncertainties are at the 2σ level.

[a]rho is the error correlation value (Ludwig, 1980)

[b]Os_i is determined based on the determined Re-Os isochron age or biostratigraphy.

[c]The three Duvernay samples are from core 1-28-36-3W5 over a 10cm interval at 3013.1m, Alberta, Canada. Regression of the Re-Os data yields a 378 ± 23 Ma with an initial ^{187}Os/^{188}Os of 0.35 ± 0.08 (MSWD = 1.6).

The Re-Os age is imprecise because of the limited spread in the ^{187}Re/^{188}Os values (~20). The Os_i values are determined at 378Ma, which agress with the biostratigraphic constraints.

[d]Three analysis from the 15cm interval of Hangenberg black shale from drill core of the Kattensiepen open cast mine, 2km north of Warstein-Suttrop, Germany (51.4668° N, 8.3975° E).

The Hangenberg Black Shale occurs below the administrative conodont Devonian-Carboniferous boundary and belongs in the upper *Praesulcata* and *Cymaclymenia nigra* Zones.

Regression of the Re-Os data yields a 366.7 ± 6.3 Ma with an initial ^{187}Os/^{188}Os of 0.42 ± 0.09 (MSWD = 0.04). Although only 3 data points, the Re-Os age is within uncertainty of the biostratigraphic constraints.

Calculating an Os_i value based on the Geologic Time Scale for the biozones of the Hangenberg black shale (~362; Ogg et al., 2008), the Os_i values become slightly more radiogenic (0.49 ± 0.02).

Background dataset for online publication only

Click here to download Background dataset for online publication only: Harris supplementary data 7_18_2013.xlsx